Cold-water coral mounds are effective carbon sinks in the western Mediterranean Sea

Luis Greiffenhagen[1], Jürgen Titschack[1], Claudia Wienberg[1], Haozhuang Wang[1,2], Dierk

5 Hebbeln[1,3]

[1] MARUM – Center for Marine Environmental Sciences, University of Bremen, Bremen, Germany

[2] State Key Laboratory of Marine Geology, Tongji University, Shanghai, China

[3] Faculty of Geosciences, University of Bremen, Bremen, Germany

10 *Correspondence to:* Luis Greiffenhagen (lgreiffenhagen@marum.de)

Abstract. Cold-water corals (CWC) build biogenic structures, so-called CWC mounds, that can store large amounts of carbon(ate). However, there is a lack of quantification studies on both recent as well as geological timescales, and knowledge is limited to the accumulation of carbonate (i.e., the inorganic carbon fraction), ignoring

15 the organic carbon fraction. This hinders the calculation of total carbon accumulation rates and a wider understanding of the role CWC mounds play in the long-term carbon cycle. Here, we investigated two cores retrieved from CWC mounds in the Alborán Sea, Western Mediterranean Sea, comprising a ~400 kyr record of carbon accumulation. We calculated the accumulation of both inorganic and organic carbon within the CWC mounds. Further, we analysed the same parameters in two cores from the adjacent seafloor (~120 kyr record) to

20 compare the mound records with the surrounding sedimentary deposits. Our results show that the studied CWC mounds accumulate up to 15 g C cm^{-2} kyr^{-1}, of which 6 – 9 % is derived from the organic carbon fraction. Moreover, during enhanced mound formation phases, the mounds store up to 14 – 19 times more carbon than the adjacent seafloor deposits. We suggest that there is a selective enrichment of organic carbon on the mounds, with about an order of magnitude higher organic carbon accumulation rates than on the adjacent seafloor. Consequently,

25 in phases of active mound formation, CWC mounds can be effective local sinks of both inorganic and organic carbon on geological timescales.

1 Introduction

Within the carbon cycle, there are two sub-cycles, the short-term and the long-term carbon cycle (Burdige, 2007;
30 Cartapanis et al., 2018). Within the world's oceans, the bulk of carbon stays in the "active", short-term cycle, while
a small fraction is buried in the sediment, that gets removed from the active system and transferred to the geological
inventory (long-term carbon cycle; Cartapanis et al., 2018). This fraction is immobilized for millions of years and
stored as organic carbon (C_{org}) or inorganic carbon (C_{inorg}; i.e., derived from calcium carbonate). Benthic carbonate
production through calcification plays a major role in this process (Ridgwell and Zeebe, 2005). As carbonate
35 factories, some calcifying organisms create biogenic structures or extensive, carbonate-rich facies over thousands
of years (Schlager, 2000; 2003; Reijmer, 2021). Quantifying their carbonate accumulation has been put into
practice (Milliman, 1974; 1993; Smith and Mackenzie, 2015; O'Mara and Dunne, 2019), however, large
knowledge gaps and high uncertainties remain (Cartapanis et al., 2018; Michel et al., 2019; Wood et al., 2023),
especially for cold-water carbonate factories. In this context, also cold-water coral (CWC) reefs in the deep sea
40 may play a significant role in the marine carbon budget (e.g., Titschack et al., 2015; Hebbeln et al., 2019; Reijmer,
2021). However, due to the particular technological difficulty to explore CWC reefs (mostly at 200 – 1200 m water
depth), knowledge about their overall role in the marine carbonate budget is still limited.

In cycles of proliferation and extinction (e.g., Dorschel et al., 2005; Roberts et al., 2009; Wienberg and Titschack,
2017), CWC reefs build so-called "CWC mounds", consisting of generations of carbonate framework-forming
45 corals growing on top of each other and stabilized by sediment infill (e.g., de Haas et al., 2009; Titschack et al.,
2009; Wang et al., 2021). Individual periods of proliferation are herein referred to as "mound formation phases".
The investigation of sediment cores taken from CWC mounds revealed that during mound formation phases, large
amounts of carbonate are accumulated (e.g., Dorschel et al., 2007b; Titschack et al., 2009). Thereby, one part of it
is derived from the coral carbonate itself, and the other part comes from pelagic and benthic carbonate buried
50 within the sediment that significantly contributes to mound formation (e.g., Titschack et al., 2009). High-resolution
3D-imagery-based core studies provide evidence that CWC mounds are substantial carbonate sinks, when
comparing their accumulation rates to the surrounding sedimentary environments (Titschack et al., 2015; 2016).
Moreover, the accumulation rates from CWC mounds are in the same range as other regional carbonate factories
such as coralline algal beds, tropical warm-water coral reefs and bryozoan facies (Titschack et al., 2015; 2016).
55 Spatially upscaled estimates of carbonate accumulation for an entire mound province suggest a significant,
regional or potentially global importance (Titschack et al., 2009; Hebbeln et al., 2019; Tamborrino et al., 2022).

Due to the limited number of carbonate accumulation rates obtained to date for CWC mounds over both time and
space (Lindberg and Mienert, 2005; Dorschel et al., 2007b; Titschack et al., 2009; 2015; 2016), CWC mounds are
still not part of global carbon(ate) budget calculations – or at least not well represented (Titschack et al., 2015;
60 Smith and McKenzie, 2016; Wood et al., 2023). Existing high-resolution studies (Titschack et al., 2015; 2016)
focus on the most recent mound formation phase. Hence, the detailed variation in carbonate accumulation across
multiple mound formation phases remains unknown. Further, all studies so far focused on the carbonate fraction
(i.e., C_{inorg}) of the carbon accumulation on CWC mounds, and there is no study that combines C_{inorg} with C_{org} to
get a holistic total mound carbon accumulation.

65 Here, we investigated ~400,000 years of CWC mound formation in the Alborán Sea, western Mediterranean.
Covering seven mound formation phases, we quantify the accumulation of C_{inorg} and C_{org} from two mounds (based
on two coral-bearing sediment cores) and provide the first total carbon accumulation rates. To provide evidence

2

for their local significance in the long-term carbon cycle and as potential sinks of C_{inorg} and C_{org}, we further compare these rates with those obtained from the adjacent seafloor (based on two coral-barren sediment cores).

70

2 Study Area

Within the Mediterranean Sea, the Alborán Sea is a hotspot of primary productivity (Morán and Estrada, 2001; Sánchez-Garrido and Nadal, 2022), CWC mound formation (Lo Iacono et al., 2009; Margreth et al., 2011; Lo Iacono et al., 2014; Stalder et al., 2018; Corbera et al., 2019; Hebbeln, 2019; Wang et al., 2019; Wienberg, 2019;
75 Corbera et al., 2021; Sánchez-Guillamón et al., 2022; Wienberg et al., 2022), and potentially, carbon burial (Masqué et al., 2003). The formation of CWC mounds in the Alborán Sea is closely linked to the flow path of the Levantine Intermediate Water (LIW) (Hayes et al., 2019). This well ventilated and nutrient-rich water mass promotes primary production as well as oxygen and food supply to the CWCs living on the mounds (Wienberg et al., 2022; Álvarez et al., 2023). In addition, the steep density gradient (pycnocline) between the low-salinity LIW
80 and the high-salinity overlying Atlantic Water (Millot, 1999) can be disturbed when it intersects a sloping topography, resulting in the formation of high-energy internal waves (e.g., Ercilla et al. 2016) that further enhance the delivery of food particles. In the southern Alborán Sea off the Moroccan margin lies the East Melilla Coral Mound Province (EMCP), which comprises various CWC mounds of very different sizes and morphologies, arising from water depths of 210 – 475 m on the upper continental slope (Fig. 1; Hebbeln 2019). Two of these
85 mounds are in the focus of this study: Brittlestar ridge I (BRI) in the north of the EMCP is an elongated ridge with a height of 140 m above the seabed, while the much smaller and shallower Dragon Mound situated ~15 km to the south of BRI arises 20 – 30 m above the seafloor (Fig. 1) with a 30 – 40 m extension below the seafloor. The CWC mounds of the EMCP developed during multiple mound formation phases (at least) since the ~Marine Isotope Stage (MIS) 11 (~390 kyr ago) until the early Holocene (see Wienberg et al., 2022 for a detailed description).
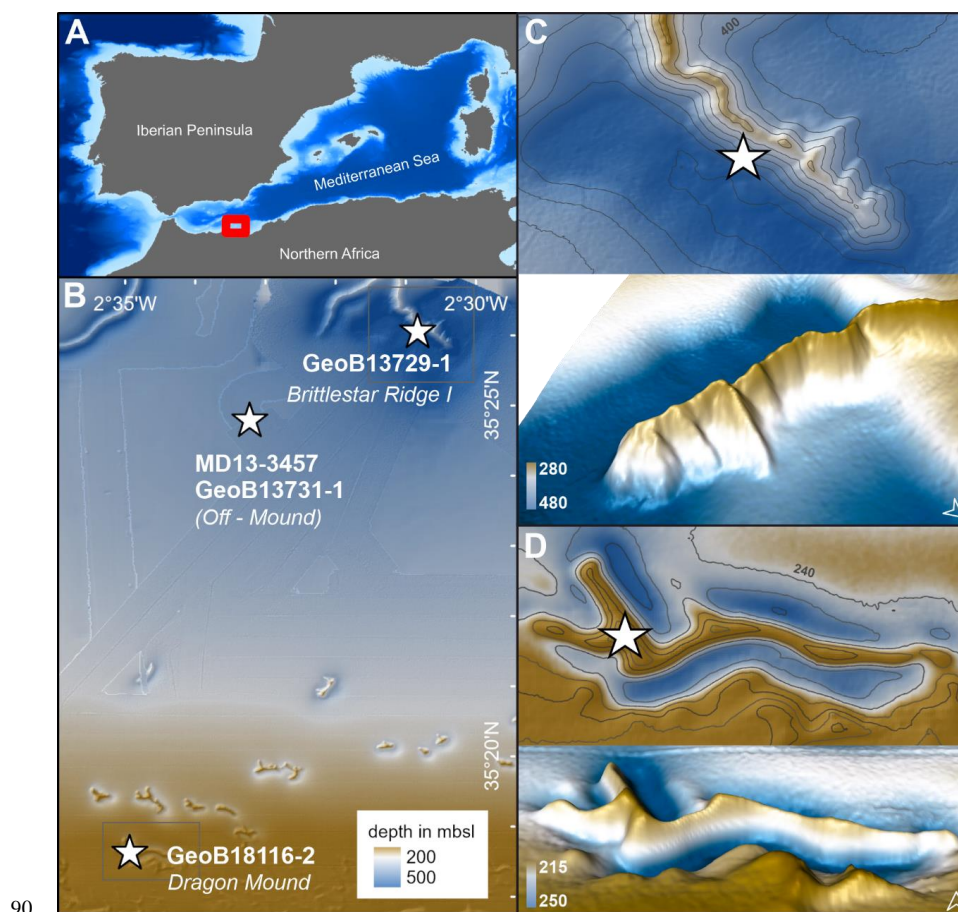
Fig. 1: Overview map the East Melilla Coral Mound Province (EMCP) showing the location of sediment cores (white stars) used in this study. B) Location of the EMCP (red box) within the western Mediterranean Sea. C) Close up 3D view of Brittlestar Ridge I, with 2D (contour lines every 25 m depth) and 3D view (3x vertical exaggeration), and D) Close up view of Dragon Mound, with 2D (contour lines every 5 m depth) and 3D view (7.5x vertical exaggeration). Maps created using ESRI ArcGIS Pro and ZIB Amira software. Bathymetry Data in A) derived from GEBCO (2024) and in B) partly supplemented by EMODnet (2022).

3 Material and Methods

This study focuses on four sediment cores collected from the EMCP in the Alborán Sea (Table 1). Two cores are taken from the CWC mounds BRI and Dragon Mound (on-mound cores), and two from the same location in the "off-mound" area between the mounds (off-mound cores; Fig. 1).

Table 1: Overview of sampling locations, corresponding coordinates, sampling depth in meters below sea level (mbsl), core recovery in meters below sea floor (mbsf), time period covered by the core,

and a description of the origin of all data (CT: computed tomography, TIC/TOC: total inorganic and organic carbon) used in this study. References [1]: Wienberg et al. **(2022), [2]: Fink** et al. **(2013), [3]: Wang** et al. **(2021), [4]: Titschack** et al. **(2016).**

Core	Location	Depth [mbsl]	Recovery [mbsf]	Age [kyr BP]	Dating	CT	TIC/TOC + Density
GeoB18116-2 *Dragon Mound*	35°18.64' N, 02°34.93' E	236	70.85	100-390	[1]	this study	this study
GeoB13729-1 *Brittlestar Ridge 1*	35°26.07' N, 02°30.83' E	442	4.47	9-12	[2; 3]	[4]	[3]
GeoB13731-1 *Off-Mound*	35°24.80′ N, 02°33.22′ E	362	4.31	0-23	[2; 3]	N/A	[3]
MD13-3457 *Off-Mound*	35°24.80′ N, 02°33.22′ E	345	20.31	0-126	this study	N/A	this study

110   The on-mound core **GeoB18116-2** was taken during *R/V Maria S. Merian* cruise MSM36 "MoccoMeBo" (Hebbeln et al., 2015) using the seafloor drill rig MeBo70 of MARUM, University of Bremen, Germany (Freudenthal and Wefer, 2013). The ~70-m-long MeBo core was retrieved from the summit of Dragon Mound in the southern part of the EMCP (Fig. 1; Table 1; Wienberg et al., 2022 for more details). MeBo drill cores are recovered in core barrels (235 cm each), which may lack sediment material (i.e., gaps in the sedimentary units)

115   due to drilling operations, or may have recoveries >100 % due to core expansion (this needs to be corrected for, using specific depth models; see Sect. 3.2). Overall, GeoB18116-2 has a recovery rate of 96 % and contains coral fragments down to ~60 – 61 m core depth (encompassing 26 core barrels), while below only fine-grained, coral-barren sediments occur (Wienberg et al., 2022). Completely penetrating a large CWC mound from the top to its base, GeoB18116-2 is a unique record in the Mediterranean Sea. Its corresponding stratigraphy covers an

120   approximate timespan between ~100 and 390 kyr BP and includes several mound formation phases (~MIS5 – MIS11; Wienberg et al., 2022).

The on-mound core **GeoB13729-1** was collected during *R/V Poseidon* cruise POS385 from BRI (Fig. 1; Hebbeln et al., 2009). The gravity core is 4.47 m long, contains coral fragments throughout and its stratigraphy refers to a timespan between 9 and 12 kyr BP (late Younger Dryas and Early Holocene; Fink et al., 2013; Wang et al., 2021).

125   For this core, we used previously published data (Table 1), based on five accelerator mass spectrometry (AMS) radiocarbon (^{14}C) coral ages, originally published by Fink et al. (2013) and 10 additional Th/U-dates published by Wang et al. (2021).

The off-mound core **GeoB13731-1** was collected during *R/V Poseidon* cruise POS385 from the adjacent seafloor within the EMCP, on the continental slope in between the two on-mound cores (10 km and 4 km distance, Fig. 1).

130   The gravity core is 4.31 m long and covers the last 23 kyr (Fink et al. 2013; Wang et al. 2021), including the mound formation phase covered in on-mound core GeoB13729-1, hence making it suitable for comparison. For this core, we use previously published data from Fink et al. (2013; 7 AMS ^{14}C ages; Table 1). From the same site, off-mound core **MD13-3457** was collected using a Calypso Corer during expedition MD194 onboard *R/V Marion Dufresne* (Van Rooij et al., 2013). With a core recovery of 20.31 m, it provides a stratigraphically longer record

135 and was therefore dated and included in the analysis to extend our comparison between on- and off-mound records towards MIS5, e.g., the latest mound formation phase covered in on-mound core GeoB18116-2.

3.1 Computed Tomography of on-mound cores GeoB18116-2 and GeoB13729-1

Computed tomography (CT) scans were performed on on-mound core **GeoB13729-1** (previously published in
140 Titschack et al., 2016) and the coral-bearing part of the MeBo core **GeoB18116-2** (upper ~60 – 61 m). The MeBo core was scanned at a resolution of 0.3 mm, using a Philips Brilliance iCT Elite 256 computer tomograph with an x-ray source voltage of 120 kV and a current of 300 mA (Klinikum Bremen-Mitte, Germany). CT data were processed using the ZIB edition of Amira Software Vers. 2022.31 (Stalling et al., 2005), closely following the approach of Titschack et al. (2015; 2016). Accordingly, the segmentation of the macrofossil fraction and the
145 sediment was set by thresholding, and all macrofossils >1 mm within the sediment were quantified. The parameters, given for each core depth at an 0.3 mm interval, include the mean x-ray attenuation in Hounsfield units (HU), and sediment and macrofossil contents in volume % (vol.%). Since the macrofossil content consists predominantly of corals, their fraction is referred to as "coral content" in the following (*sensu* Titschack et al., 2016). The data points corresponding to the outlined parameters were averaged to a 5 cm resolution, using a
150 running average function. In the specific case of the MeBo core GeoB18116-2, each core barrel (n= 26; each ~235 cm in length including a core catcher) was treated individually. CT orthoslice images, 3D clast quantification, clast size, clast orientation and coral content, mean x-ray attenuation and its standard deviation (SD) are presented for each core barrel, along with its corresponding depth in the Supplementary Material.

155 3.2 Depth Model of MeBo core GeoB18116-2 (Dragon Mound)

For the purpose of this study, a new depth model was introduced that compensates for core expansion (>100% recovery) in MeBo core **GeoB18116-2**, following the IODP Core depth below Sea Floor B (CSF-B; IODP depth scales terminology standards IODP, 2011). This new depth model results in some minor depth differences compared to the depth model of Wienberg et al. (2022), which followed the Core depth below Sea Floor A (CSF-
160 A) standard of IODP, and results in some minor differences in the calculated mound aggradation rates (ARs). While CSF-A refers to the drill depth based on actual core barrel length, this study requires the use of CSF-B, that uses a compression algorithm (i.e., linear squeeze) of the core barrel length to 100% recovery. This is necessary to assign more accurate depths to the data points obtained from the CT scan. Gaps in the sediment record (void air spaces) were also subtracted from the record, and not counted as depth (CSF-B). In addition, several section tops
165 showed an unusually high coral content for the first ca. 5 cm. This is an effect specific to Me-Bo drilling, where core barrels are separately retrieved from the drill holes. As this may cause core breccia falling into the drill hole in between drilling sections, i.e., coral fragments, the corresponding data are considered inaccurate and were subsequently removed from the depth record and assigned "no data". The depth models are made available in the PANGAEA open data repository. In the following all core depths of GeoB18116-2 refer to the CSF-B depth model.

170

6

3.3 Age Models

For core **GeoB18116-2** (Dragon Mound), all coral ages (n= 76) and the derived mound formation phases and mound ARs are based on Th/U-dating of the scleractinian CWC *Lophelia pertusa* and were previously published by Wienberg et al. (2022). Coral ages range from 390 to 103 kyr BP, and were assigned to six mound formation

175   phases (DM1 to DM6; each corresponding to one AR), see Wienberg et al. (2022) for more detail. The mound formation phases are separated by hiatuses, i.e., periods without any CWC mound formation which span remarkably long time periods of 10 – 90 kyr (Wienberg et al. 2022). Except for DM2 (~MIS10; glacial), all pronounced mound formation phases on Dragon Mound clearly correspond to interglacial periods. Notably, several coral ages between ~20 and 27 m core depth are scattered across a large time span covering MIS7d – MIS9,

180   which results in low ARs of <15 cm kyr^{-1}. Accordingly, this low aggradation period (DM4) was classified as a period of slow mound formation, i.e., scarce reef growth, following Frank et al. (2009). Due to the CT-based high-resolution imagery and based on sudden changes in coral content, coral fragment orientation and matrix sediment density (see Supplementary Material), the exact position of mound formation phase boundaries were determined resulting in slightly adapted boundary depths and ARs compared to Wienberg et al. (2022). The depth of the mound

185   base is slightly deeper than the deepest obtained coral age, consequently the AR for DM1 during MIS11 is likely underestimated.

The age model of on-mound core **GeoB13729-1** (Brittlestar Ridge I), is based on five accelerator mass spectrometry (AMS) radiocarbon (^{14}C) coral ages, originally published by Fink et al. (2013) and 10 additional Th/U-dates published by Wang et al. (2021). This study used the age model of Wang et al. (2021). The record

190   documents one mound formation phase between 9 and 12 kyr BP, which is the last of several mound formation phases on BRI (Fentimen et al., 2020; Wienberg et al., 2022; Fentimen et al., 2022). This phase will hereafter be referred to as "BRI$_{final}$". Notably, BRI$_{final}$ is also documented in several other cores collected from BRI (Fink et al., 2013; Stalder et al., 2018; Fentimen et al., 2020; Fentimen et al., 2022; Wienberg et al., 2022; Fentimen et al., 2023; Korpanty et al., 2023), pointing out that BRI$_{final}$ started earlier than documented in core GeoB13729-1.

195   However, Wienberg et al. (2022), who investigated the entire phase covering coral ages from 15 – 8 kyr BP found overall ARs of 130 – 140 cm kyr^{-1} which matches well with the AR for BRI$_{final}$ used in this study (135 cm kyr^{-1}; Wang et al., 2021), supporting the use of GeoB13729-1 for our purposes, despite not covering the entire mound formation phase with our record.

The age model of off-mound core **MD13-3457** is based on eight AMS ^{14}C ages obtained from mixed planktonic

200   foraminifera. Measurements were performed on >15 mg of planktonic foraminifera >150 µm at the Poznan Radiocarbon Laboratory, Poland. Additionally, the stable oxygen isotope (δ^{18}O) composition of the epi-benthic foraminifera *Cibicidoides mundulus* was analysed for ~10 specimens in the same size fraction at a 5 cm core resolution to extend the age model of MD13-3457. Measurements were performed using a Finnigan MAT 252 gas isotope ratio mass spectrometer connected to a Kiel II automated carbonate preparation device at the MARUM,

205   University of Bremen, Germany, following Vienna Pee Dee Belemnite and NBS 19 standards (±0.09‰ δ^{18}O standard deviation). For the age model of core **GeoB13731-1**, seven previously published AMS ^{14}C ages were used (Fink et al., 2013; Wang et al., 2021).

For both off-mound cores, age models were produced with the Undatable software (Vers. 1.31, Lougheed and Obrochta, 2019) in Matlab (R2021b Vers. 7), using 10^5 Monte Carlo iterations of age uncertainty sampling. AMS

210   ^{14}C ages from both off-mound cores were calibrated using the IntCal20 calibration curve (Reimer et al., 2020) and

modelled reservoir ages of Butzin et al. (2017) extracted with Palaeo Data View (PDV) software (Langner and Mulitza, 2019). For core MD13-3457, additional tie points were set in PDV by comparing the global benthic LR04 stack (Lisiecki and Raymo, 2005) with our $\delta^{18}O$ record. The age error of the tie points was conservatively set at 4 kyr, since this is the estimated uncertainty of the benthic stack curve of Lisiecki and Raymo (2005) for 1 Myr until

215 present.

Sedimentation rates were calculated using a linear interpolation between the calibrated ages (and tie points) for both cores (see supplementary material for more detail). By working with a consistent methodology for both off-mound cores, we provide a first age model of core MD13-3457, and update the age model of core GeoB13731-1 (cf. Wang et al., 2021).

220

3.4 Matrix Sediment Dry Bulk Density Measurements

Sediment samples of 6-10 cm^3 were taken from the on-mound core **GeoB18116-2** and the off-mound core **MD13-3457** to determine dry bulk densities (DBDs). DBD data from on-mound core **GeoB13729-1** (n= 22) and off-mound core **GeoB13731-1** (n= 22) were generated by Wang et al. (2021) following the same procedure as outlined

225 below (data available at: https://doi.pangaea.de/10.1594/PANGAEA.941018).

Samples from core **GeoB18116-2** were collected at the approximate beginning and end of each mound formation phase (n= 18; range: 1.17 – 1.40 g cm^{-3}). The off-mound core **MD13-3457** was sampled for DBD measurements at an equal distance of every meter (n= 21; range: 0.88 – 1.44 g cm^{-3}). The DBD measurements were performed following ODP standards (Blum, 1997). Samples were dried for 24h at 105 °C, and their weight was measured

230 before and after. Then, dry sediment volumes were determined using a PentaPyc 5200e gas pycnometer (Quantachrome instruments) in the Geotechnical Laboratory at MARUM, University or Bremen, Germany. Since GeoB18116-2 has been scanned by CT, we then followed an additional approach for this core: As CT x-ray attenuation data have been used as a proxy for DBD in the past (Orsi et al., 1994; Gerland and Villinger, 1995; Orsi and Anderson, 1999; Duchesne et al., 2009) and observing a high linear correlation ($R^2 = 0.89$; p-val. = <

235 0.0001) between DBD and x-ray attenuation data throughout GeoB18116-2 (see supplementary material for calibration details), we calculated DBD values from the x-ray attenuation data for core GeoB18116-2. This highly increased the resolution of our sediment density data, and may be an alternative, non-invasive and time-efficient methodology to obtain density data for similar purposes.

240 **3.5 Total Organic and Inorganic Carbon Analysis**

Sediment samples of 6-10 cm^3 were collected from on-mound core **GeoB18116-2** and off-mound core **MD13-3457** to measure the total organic carbon (TOC) and total inorganic carbon (TIC) content. TIC/TOC data from cores **GeoB13729-1** (n= 44) and **GeoB13731-1** (n= 43) were obtained by Wang et al. (2021) at 10 and 5 cm resolution, respectively, following the same procedure as outlined below (data available at:

245 https://doi.pangaea.de/10.1594/PANGAEA.941018).

Samples from the on-mound core **GeoB18116-2** (n= 54) were collected at core levels corresponding to roughly comparable age intervals. Off-mound core **MD13-3457** was sampled every 10 cm (n= 169) from core depth 355 cm downwards, to account for the record that is not already covered by the off-mound core GeoB13731-1.

Macrofossil fragments of ca. >2 mm were removed from the sample to avoid misrepresentation of the sediment
250 fraction, before the freeze-dried samples were ground. From each sample, one sub-sample (~100 mg) was analysed
for TC, and one for TOC after it was treated with hydrochloric acid to remove carbonate. Measurements were
performed with a LECO CS 744 at the Department of Geosciences, University of Bremen, Germany.
Subsequently, the TIC content was calculated as TIC = TC – TOC, all given in weight percent (wt.%).

3.6 Methods of Calculating Carbon(ate) Accumulation

255

We calculated the ***total carbon accumulation***, which consists of three different carbon fractions: A) the ***coral
inorganic carbon*** accumulation (coral C_{inorg} Acc), specific to the on-mound cores, B) the ***sediment inorganic
carbon*** accumulation (sediment C_{inorg} Acc), and C) the ***sediment organic carbon*** accumulation (sediment C_{org}
Acc).

260

Coral Inorganic Carbon Accumulation

Coral C_{inorg} Acc for core **GeoB18116-2** (Dragon Mound) was first calculated at 5 cm core resolution (1138 data
points, spanning the upper 61.27 m (CSF-B), closely following the methodology outlined in Titschack et al. (2015;
2016). Thereby, a coral density of 2.66 g cm^{-3} (i.e., 100% carbonate; Dorschel et al., 2007b) was multiplied with
265 the *coral content* (vol.%) from the CT data. Combined with the corresponding mound ARs [cm kyr^{-1}], coral
carbonate accumulation [g CaCO$_3$ cm^{-2} kyr^{-1}] was determined for each 5 cm-average depth point (Eq. 1).

$$coral\ C_{inorg}\ Acc\ \frac{g}{cm^2 \times kyr} = Coral\ Vol.\% \times Coral\ Density\ \frac{g}{cm^3} \times Aggradation\ Rate\ \frac{cm}{kyr} \times \frac{12.01}{100.09} \quad \textbf{(1)}$$

Accounting for the molecular weight fraction of carbon within carbonate (i.e., 12% C in CaCO$_3$; see Eq. 1), coral
carbonate accumulation was converted to coral C_{inorg} Acc. On-mound core **GeoB13729-1** was handled the same
270 way using CT data from Titschack et al. (2016), covering the interval of 0.05 – 4.25 m (43 data points), combined
with the age model and sediment density data published in Wang et al. (2021).

Sediment Organic and Inorganic Carbon Accumulation

The calculation of **sediment C_{inorg} Acc** and **sediment C_{org} Acc** is based on the C_{inorg} and C_{org} wt.% contents
275 resulting from the obtained TIC/TOC data (Sect. 3.5) on the matrix sediments.

$$sed.\ C_{(in)org}\ Acc\ \frac{g}{cm^2 \times kyr} = \frac{TIC}{TOC} wt.\% \times sed.\ Vol.\% \times sed.\ Density\ \frac{g}{cm^3} \times Aggradation\ Rate\ \frac{cm}{kyr} \quad \textbf{(2)}$$

The sediment C_{org} and C_{inorg} contents were multiplied by the CT-derived matrix sediment volume % (in case of the
coral-bearing on-mound cores, since only part of the total volume consists of matrix sediment). Then, each data
point was assigned a matrix sediment DBD value ([g cm^{-3}]; based on linear interpolation or, if available, CT
280 calibration, Sect. 3.4) at the given depth and multiplied. Each of the core depths with C_{org} and C_{inorg} values [g cm^{-3}]
were then assigned to a corresponding AR, and multiplied again. Eventually, this results in both a sediment C_{inorg}
and C_{org} Acc [g C cm^{-2} kyr^{-1}], see Eq. 2. This was calculated for both CWC-bearing cores and both off-mound
records for comparison. Sediment C_{inorg} [g cm^{-3}] may also be converted to carbonate using the molecular weight

share described above, in order to describe the total carbonate accumulation (coral carbonate + sediment
carbonate).

Total Carbon Accumulation

To determine the **total carbon accumulation** (Eq. 3) for the studied CWC mounds, the CT-based coral C_{inorg} Acc data points were downscaled to the resolution of the C_{org} and C_{inorg} data (i.e., 54 data points for core GeoB18116-2; 44 data points for core GeoB13729-1 from the TIC/TOC measurements). Then, all data points within a mound formation phase were averaged and mean, minimum and maximum values per mound formation phase are provided for total carbon accumulation, coral C_{inorg} Acc, sediment C_{inorg} Acc, and sediment C_{org} Acc. Additionally, we present the same for carbon*ate* accumulation (total carbonate accumulation, i.e., coral carbonate and sediment carbonate accumulation). Ultimately, we obtain the relative contribution (%) of each carbon fraction to the total carbonate and total carbon accumulation.

$$C_{total}\ Acc\ \ \frac{g}{cm^2 \times kyr} = coral\ C_{inorg}\ Acc\ +\ sediment\ C_{inorg}\ Acc\ +\ sediemnt\ \ C_{org}\ Acc \qquad (3)$$

The total carbon accumulation was also obtained for both off-mound cores (sediment C_{inorg} Acc and sediment C_{org} Acc). Here, we present weighted-mean values of accumulation rates from the off-mound core corresponding to a specific mound formation phase in the on-mound cores. This facilitates a comparison of mean carbon accumulation between on- and off-mound settings during the same time interval (Table 1). While samples from core GeoB13731-1 (9 – 12 kyr BP; n= 6) were used to compare the carbon accumulation rates with the latest mound formation phase (BRI$_{final}$) (GeoB13729-1; n= 43), core MD13-3457 (108 – 115 kyr BP; n = 10) was used to compare with the latest mound formation phase (DM6) preserved in Dragon Mound (GeoB18116-2; n= 9). All parameters from the off-mound cores were averaged and compared with regards to that exact timespan, rounded up to kyr scale (for raw data beyond the period of DM6 in off-mound core MD13-3457, please refer to data sets published in Pangaea and the supplementary material).

4 Results

4.1 On-Mound Carbon(ate) Accumulation

4.1.1 Dragon Mound Record: Results from a 61 m long CT scan

The visual inspection of the CT scans revealed that the coral content of core GeoB18116-2 was mainly composed of *Lophelia pertusa*, with minor contributions of dendrophylliid corals. The average coral content is 14 vol.% (5 cm average) with a maximum of 42 vol.% for core sections with high coral content (Fig. 2a). There are no major coral-barren units, and some clearly visible hiatuses (Fig. 2b). The mound base lies at ~61.1 mbsf (CSF-B depth; Fig. 2c).
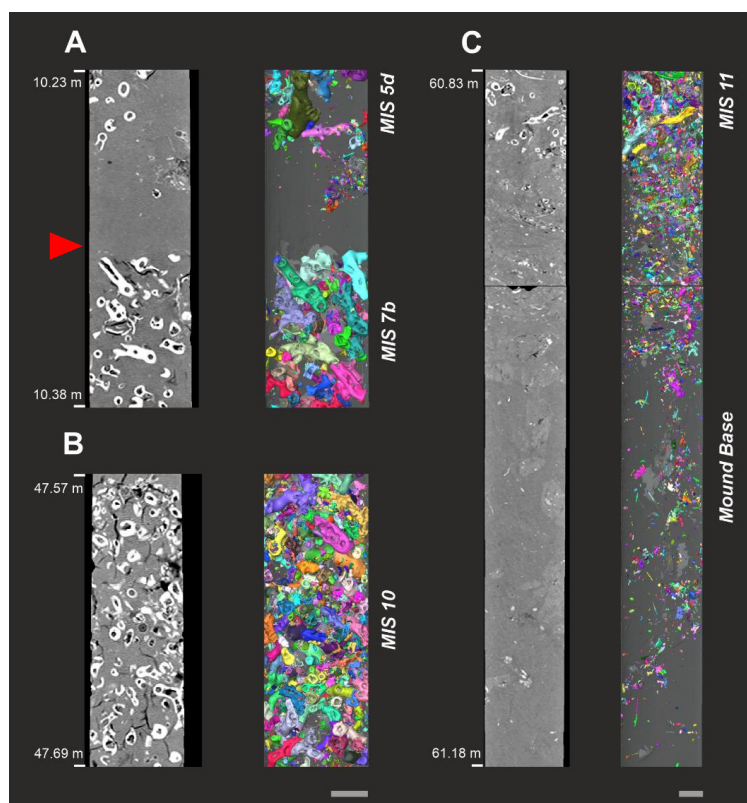
Fig. 2: CT-image based core section close-ups of the MeBo on-mound core GeoB18116-2 collected from Dragon Mound (left: orthoslice; right: 3D macrofossils reconstruction, each coral fragment with individual color; core depth given in CSF-B meters below seafloor). (A) Hiatus covering a timespan of ~100 kyr between mound formation phases DM5 and DM6, red arrow indicating the top of DM5 (coral ages ~MIS7b), followed by DM6 (corals ages ~MIS5d). (B) Example of a high-coral carbonate-bearing unit during mound formation phase DM2 (MIS10, ~350 kyr BP). (C) Scan of the mound base (61.1 mbsf), including few bioturbations, the first CWC clasts and several oyster shells, DM1 (~MIS11). Grey scale bars on the bottom represent ~2 cm length.

Based on the CT-derived localisation of mound formation phase boundaries and considering the new core depth model (CSF-B), the newly calculated ARs of the individual mound formation phases deviate slightly from those previously published by Wienberg et al. (2022; cf. Table 2). The mound initiation phase DM1 (~MIS11) shows an AR of 22 cm kyr^{-1}, followed by DM2 and DM3 (~MIS9b-d and MIS10), corresponding to an AR of 61 cm kyr^{-1} each. The slow mound formation phase DM4 (~MIS7d – MIS9) has an AR of 11 cm kyr^{-1}, during DM5 (~MIS7b) ARs amount to 131 cm kyr^{-1}, and the most recent mound formation phase DM6 (~MIS5d) has the highest AR with 147 cm kyr^{-1} (Fig. 3; Table 2).

11

For further details on all core raw data results (DBD, TIC/TOC and CT coral volumes, CT raw data and obtained

335   off-mound AMS ^{14}C ages) that fed into the calculation of carbon accumulation rates, please refer to the

supplementary material and PANGAEA open data repository.

4.1.2 Carbonate Accumulation Rates

Total mean on-mound carbonate accumulation rates, averaged across each defined mound formation phases from

340   the sediment cores collected from Dragon Mound and BRI, lie between $49 - 115$ g $CaCO_3$ cm^{-2} kyr^{-1} for DM2,

DM3, DM5, DM6 and BRI$_{final}$ (Fig. 3, Table 2). Exhibiting mean rates of $105 - 115$ g $CaCO_3$ cm^{-2} kyr^{-1} (range: 71

$- 167$ g $CaCO_3$ cm^{-2} kyr^{-1}), the youngest "enhanced" mound formation phases (DM5, DM6 and BRI$_{final}$) are all in

the same range, and more than twice as high as the rates from the earlier mound formation phases (DM2 and DM3)

that show mean rates of 49 and 53 g $CaCO_3$ cm^{-2} kyr^{-1} (range: $32 - 66$ g $CaCO_3$ cm^{-2} kyr^{-1}). The mound initiation

345   phase DM1 as well as the slow mound formation phase DM4 show much lower rates, with 16 and 11 g $CaCO_3$

cm^{-2} kyr^{-1} (range: $9 - 19$ g $CaCO_3$ cm^{-2} kyr^{-1}), respectively. Overall, the contribution of the coral carbonate fraction

to the total mound carbonate accumulation (Fig. 3, Table 2) varies between 32 % and 56 % (DM1 and BRI$_{final}$,

respectively) throughout the mound formation phases. Accordingly, the carbonate derived from the sediment

matrix (sediment carbonate) contributes $44 - 68$ % to the total mound carbonate accumulation.

350

355

360

365

Table 2: All rates of mound aggradation (AR), carbonate accumulation (Acc) and fraction contribution (%) per mound formation phase (Brittlestar Ridge I: BRI$_{final}$, Dragon Mound: DM6 – DM1) for coral- and sediment-derived carbonate. The minimum – maximum range is given in brackets (light grey). Column "age" indicates the duration of mound formation phase based on coral ages. Column "period" indicates the approximate corresponding marine isotope stage (MIS).
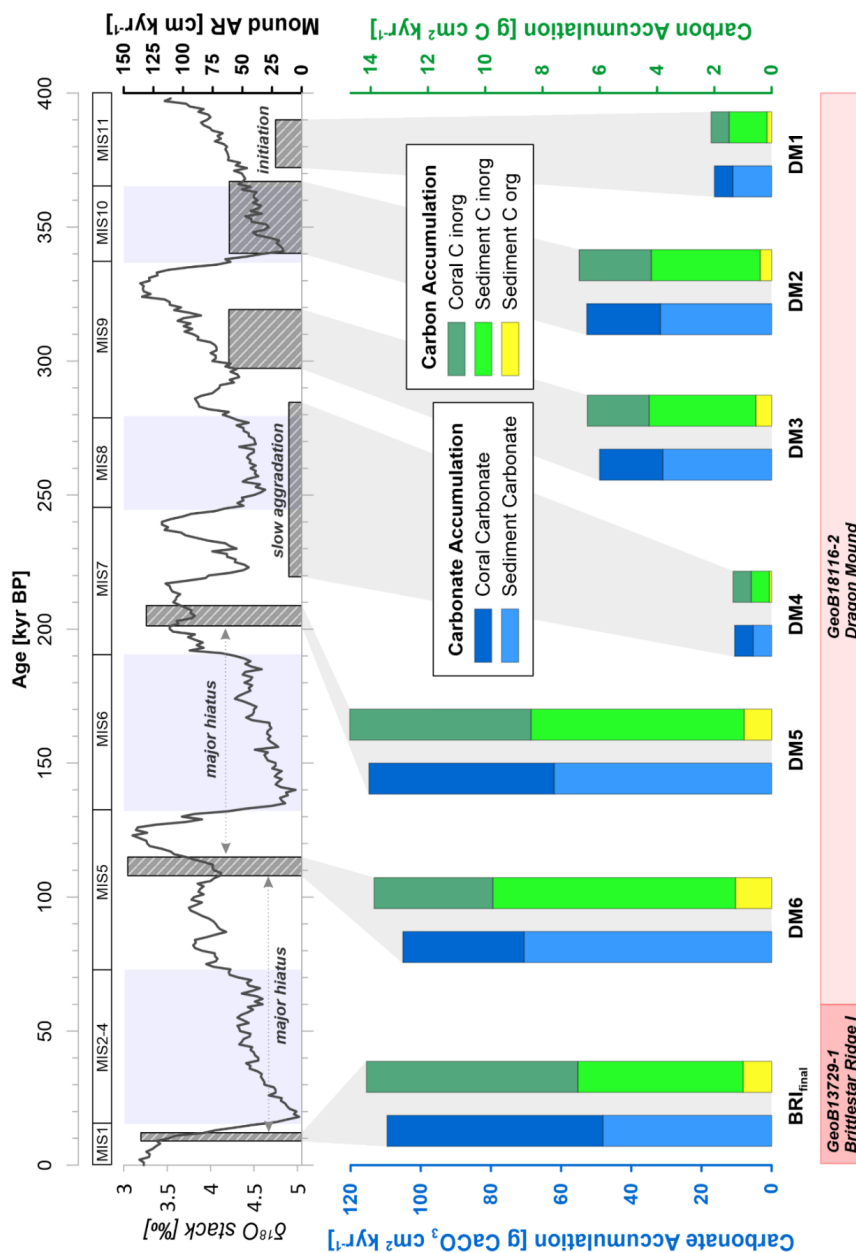
Mound Formation Phases	Age [kyr BP]	Period [MIS]	AR [cm kyr⁻¹]	Total Carbonate Acc [g CaCO₃ cm⁻² kyr⁻¹]	Coral Carbonate Acc [g CaCO₃ cm⁻² kyr⁻¹]	%	Sediment Carbonate Acc [g CaCO₃ cm⁻² kyr⁻¹]	%
Brittlestar Ridge I (GeoB13729-1)								
BRI$_{final}$	9-12	MIS1	135	110 (71-167)	61.5 (21-127)	56	48.1 (39-57)	44
Dragon Mound (GeoB18116-2)								
DM6	108-115	MIS5d	147	105 (86-144)	34.6 (12-73)	33	70.6 (68-73)	67
DM5	201-208	MIS7b	131	115 (87-142)	52.8 (14-86)	46	62.0 (52-73)	54
DM4	220-285	MIS7d-9	11	11 (9-12)	5.3 (4-7)	50	5.3 (4-6)	50
DM3	297-319	MIS9b-d	61	49 (38-56)	18.0 (2-26)	37	31.0 (28-36)	63
DM2	340-367	MIS10	61	53 (32-66)	21.0 (2-37)	40	31.7 (25-38)	60
DM1	372-390	MIS11	22	16 (15-19)	5.2 (3-8)	32	11.1 (10-12)	68

Table 3: All rates of mound aggradation (AR), mound carbon accumulation (Acc) and contribution (%) per mound formation phase (Brittlestar Ridge I: BRI$_{final}$, Dragon Mound: DM6 – DM1) for coral- and sediment-derived inorganic carbon (Coral C$_{inorg}$, Sediment C$_{inorg}$), plus the organic carbon fraction from the mound sediment (Sediment C$_{org}$) to the total carbon accumulation. The minimum – maximum range is given in brackets (light grey). Column "age" indicates the duration of the mound formation phase based on coral ages. Column "period" indicates the approximate corresponding marine isotope stage (MIS).

Mound Formation Phases	Age [kyr BP]	Period [MIS]	AR [cm kyr⁻¹]	Total Carbon Acc [g C cm⁻² kyr⁻¹]		Coral C$_{inorg}$ Acc [g C cm⁻² kyr⁻¹]		%	Sediment C$_{inorg}$ Acc [g C cm⁻² kyr⁻¹]		%	Sediment C$_{org}$ Acc [g C cm⁻² kyr⁻¹]		%
Brittlestar Ridge I (GeoB13729-1)														
BRI$_{final}$	9-12	MIS1	135	14.1	(10-21)	7.38	(2.5-15.2)	52	5.77	(4.7-6.9)	41	0.99	(0.6-1.2)	7
Dragon Mound (GeoB18116-2)														
DM6	108-115	MIS5d	147	13.9	(12-18)	4.15	(1.5-8.8)	30	8.47	(8.2-8.8)	61	1.26	(0.9-1.5)	9
DM5	201-208	MIS7b	131	14.7	(12-18)	6.33	(1.6-10.4)	43	7.44	(6.2-8.8)	51	0.96	(0.7-1.2)	6
DM4	220-285	MIS7d-9	11	1.3	(1.1-1.6)	0.63	(0.4-0.8)	47	0.63	(0.5-0.7)	47	0.08	(0.06-0.10)	6
DM3	297-319	MIS9b-d	61	6.4	(5.1-7.1)	2.16	(0.3-3.2)	34	3.72	(3.3-4.3)	58	0.55	(0.4-0.7)	8
DM2	340-367	MIS10	61	6.7	(4.2-8.3)	2.52	(0.2-4.4)	37	3.81	(3.0-4.6)	57	0.40	(0.3-0.5)	6
DM1	372-390	MIS11	22	2.1	(2.0-2.4)	0.63	(0.3-1.0)	30	1.33	(1.2-1.5)	63	0.16	(0.1-0.2)	7

Fig. 3: Illustration of the carbonate accumulation (blue tone colours) and carbon accumulation (green-yellow colours) for Dragon Mound and Brittlestar Ridge I (BRI), based on each mound formation phase (Brittlestar Ridge I: BRI$_{final}$, Dragon Mound: DM6 – DM1), Mound formation phases (duration to scale) and aggradation rate shown in the top graph. Top x-axis provides a timescale, and corresponding global climate variations according to the benthic δ^{18}O stack by Lisiecki and Raymo (2005), with marine isotope stages (MIS) indicated above. Glacial periods are highlighted by light blue bars. Bottom graph showing the contribution of each carbon(ate) fraction to the total. Note that the bar width for the lower graph has no timescale, and carbonate and carbon accumulation rates are scaled to different axes (left and right y-axis, respectively).

4.1.3 Carbon accumulation rates

430   Total mean mound carbon accumulation rates, averaged across the defined mound formation phases, amount to 6 – 15 g C cm^{-2} kyr^{-1} for DM2, DM3, DM5, DM6 and BRI$_{final}$ (range 4 – 21 g C cm^{-2} kyr^{-1}; Fig. 3, Table 3). Analogous to the carbonate accumulation, the three most recent mound formation phases show a comparable total carbon accumulation rate of 14 – 15 g C cm^{-2} kyr^{-1} (range 10 – 21 g C cm^{-2} kyr^{-1}), while during DM2 and DM3 accumulation was ~50% lower (mean 6 and 7 g C cm^{-2} kyr^{-1}, respectively; range: 4 – 8 g C cm^{-2} kyr^{-1}). During the

435   slow mound formation phase (DM4) and the Dragon Mound initiation phase (DM1), only 1.3 – 2.1 g C cm^{-2} kyr^{-1} (range: 1.1 – 2.4 g C cm^{-2} kyr^{-1}) were accumulated.

The C$_{inorg}$ Acc accounts for the largest contribution to total carbon accumulation here, with coral C$_{inorg}$ varying between 30 – 52 %, and sedimentary C$_{inorg}$ between 41 – 63 %. The sedimentary C$_{org}$ fraction contributes, with 0.1 – 1.3 g C cm^{-2} kyr^{-1} (range: 0.1 – 1.5 g C cm^{-2} kyr^{-1}), 6 – 9 % to the total mound accumulation amongst the studied

440   sites. For all carbon fractions individually, DM5, DM6 and BRI$_{final}$ exhibit the highest values in accumulation, by a factor of ~2 higher than during DM2 and DM3, which in turn, exceed DM1 and DM4 by a factor of ~2 (Fig. 3, Table 3).

4.2 Off-mound carbon(ate) accumulation rates

445   During BRI$_{final}$, the off-mound record GeoB13731-1 accounts for a mean sedimentation rate (SR) of 16 cm kyr^{-1}, and a total mean carbonate accumulation of 7.25 g CaCO$_3$ cm^{-2} kyr^{-1} (range: 4.17 – 9.83 g CaCO$_3$ cm^{-2} kyr^{-1}; based on data from Wang et al., 2021). The total mean carbon accumulation accounts for 0.99 g C cm^{-2} kyr^{-1} (range: 0.56 – 1.33 g C cm^{-2} kyr^{-1}), comprised of a sediment C$_{org}$ Acc of 0.11 g C cm^{-2} kyr^{-1} (range: 0.05 – 0.16 g C cm^{-2} kyr^{-1}), and a sediment C$_{inorg}$ Acc of 0.87 g C cm^{-2} kyr^{-1} (range: 0.50 – 1.18 g C cm^{-2} kyr^{-1}; based on data from Wang et al.,

450   2021).

During DM6, the off-mound record MD13-3457 accounts for a mean sedimentation rate of 12 cm kyr^{-1}, and a mean carbonate accumulation rate of 5.50 g CaCO$_3$ cm^{-2} kyr^{-1} (range: 3.83 – 7.25 g CaCO$_3$ cm^{-2} kyr^{-1}). The total mean carbon accumulation accounts for 0.75 g C cm^{-2} kyr^{-1} (range: 0.52 – 0.98 g C cm^{-2} kyr^{-1}) comprised of sediment C$_{org}$ Acc of 0.09 g C cm^{-2} kyr^{-1} (range: 0.06 – 0.12 g C cm^{-2} kyr^{-1}) and a sediment C$_{inorg}$ Acc of 0.66 g C

455   cm^{-2} kyr^{-1} (range: 0.46 – 0.87 g C cm^{-2} kyr^{-1}).

4.3 On-Mound versus Off-Mound Carbon Accumulation Rates

The comparison of synchronously deposited off-mound (GeoB13731-1 and MD13-3457) with the on-mound core sequences (GeoB13729-1 and GeoB18116-2) for the last two periods of mound formation reveals contrasting

460   carbon contents and accumulation rates (Fig. 4; Table 4).
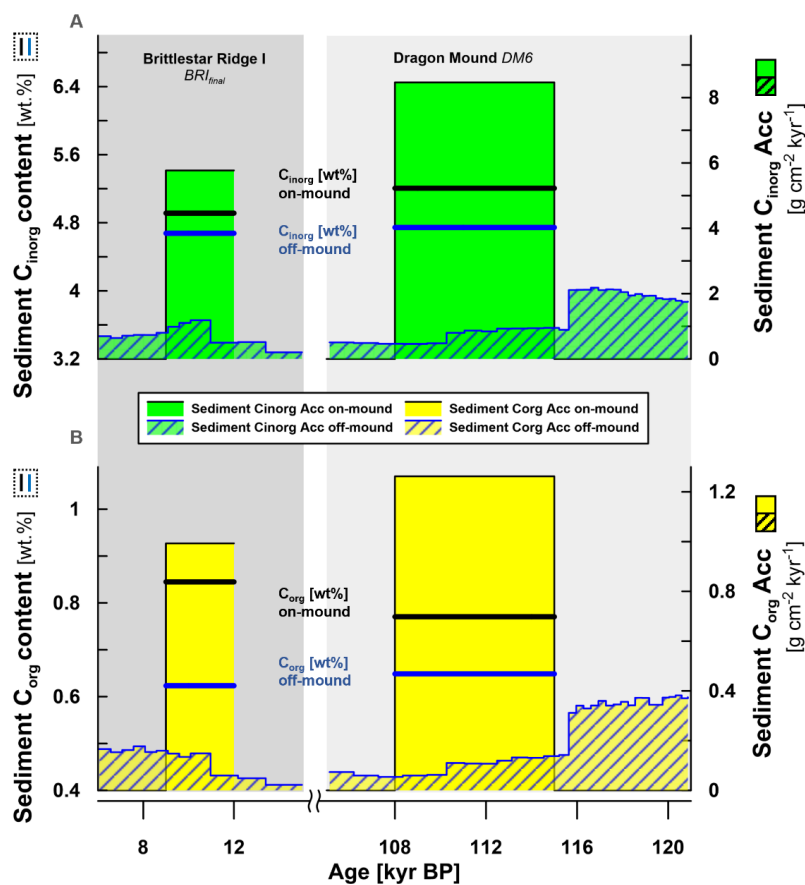
Fig. 4: Comparison of sediment C_{inorg} and C_{org} contents [bold lines, wt. %; left y-axes] and accumulation (Acc) rates [filled bars, g C cm^{-2} kyr^{-1}; right y-axes] between on- and off-mound cores, focusing on two mound formation phases (timespan see x-axis) with BRI_{final} on Brittlestar Ridge I corresponding to MIS1 (background highlighted in dark grey; GeoB13729-1 and GeoB13731-1); and DM6 on Dragon Mound corresponding to MIS5 (background highlighted in light grey; GeoB18116-2 and MD13-3457). A) All C_{inorg} data in the top half (*green*), B) All C_{org} data are shown in the bottom half (*yellow*). All off-mound data have a *blue* colour outline, all on-mound data have a *black* colour outline. Carbon accumulation rates shown as *bars*, carbon contents shown as *line*. Rates of on-mound record shown as mean per mound formation phase. Rates of off-mound record shown at TIC/TOC sample resolution including the trend prior to and after the corresponding mound formation phase. For comparison, the mean C_{org} and C_{inorg} contents are displayed too. Note x-axis break (15 – 105 kyr BP) between mound formation phases.

During the mound formation phase BRI_{final}, the sediment C_{org} content (wt.%) is about 1.4 times higher on the CWC mound, compared to the off-mound record (Fig. 4, Table 4). During the mound formation phase DM6, the sediment

C_{org} content is about 1.2 times higher on the mound. The mean sediment C_{inorg} contents just slightly higher on the CWC mounds, compared to the off-mounds (ratio 1.1 for both periods). Hitherto, all mean carbon content values

480 (sediment C_{org} and sediment C_{inorg}) are higher on the mounds.

Table 4: All core data from the mound formation phases BRI$_{final}$ (documented in core GeoB13729-1; Brittlestar Ridge I, i.e. BRI), and DM6 (documented in core GeoB18116-2; Dragon Mound), each compared to the corresponding time interval measured in the off-mound cores GeoB13731-1 and

485 **MD13-3457, respectively. Columns show organic carbon content (C_{org}), inorganic carbon (C_{inorg}) content, mound aggradation (AR) / sedimentation rate for the off-mound core (SR), carbon accumulation (Acc). Ratio indicates the factor by which the CWC mounds exceeds the off-mound record (i.e., on-mound : off-mound).**

	C_{org} [wt.%]	$C_{inorg.}$ [wt.%]	AR or SR [cm kyr^{-1}]	Total Carbon Acc [g C cm^{-2} kyr^{-1}]	C_{inorg} Acc [g C cm^{-2} kyr^{-1}]		Sediment C_{org} Acc [g C cm^{-2} kyr^{-1}]
					Sediment	Total	
9 - 12 kyr BP							
BRI	0.84	4.91	135	14.1	5.77	13.16	0.99
Off-Mound	0.62	4.68	16	1.0	0.87	0.87	0.11
ratio	*1.4*	*1.1*	*8.5*	*14.3*	*6.6*	*15.1*	*8.7*
108 - 115 kyr BP							
DM6	0.77	5.21	147	13.9	8.47	12.62	1.26
Off-Mound	0.65	4.75	12	0.8	0.66	0.66	0.09
ratio	*1.2*	*1.1*	*12.6*	*18.5*	*12.8*	*19.1*	*14.0*

490 The difference between on- and off-mound records becomes clearer when comparing the accumulation rates during the same time period (Fig. 4, Table 4). Most importantly, all carbon accumulation rates during BRI$_{final}$ and DM6 are around one order of magnitude higher compared to the off-mound cores GeoB13731-1 and MD13-3457. During the mound formation phases BRI$_{final}$ and DM6, the sediment C_{org} Acc is 9 and 14 times higher on the CWC mounds than in the off-mound records, respectively. The sediment C_{inorg} Acc on the mounds exceeds the off-

495 mound records by factors of 7 (BRI$_{final}$) and 13 (DM6).

These factors increase to 15 (BRI$_{final}$) and 19 (DM6), when also accounting for the coral C_{inorg} Acc in the on-mound records, due to the lack of coral macrofossils in the off-mound setting. The total carbon accumulation (coral C_{inorg} + sediment C_{inorg} + sediment C_{org} Acc) on the mounds is 15 (BRI$_{final}$) and 19 (DM6) times higher (Fig. 4, Table 4), compared to the off-mound environment during the same period, e. g. 9 – 12 kyr BP and 108 – 115 kyr BP.

500 The data presented in figure 4 show contrasting trends for off-mound sediment C_{org} Acc between the mound formation phases. During and after BRI$_{final}$, off-mound C_{org} Acc increases, while before and throughout DM6, values decrease. At the same time, C_{inorg} Acc during BRI$_{final}$ first increases in the off-mound record, but then show a sudden drop that continues after mound formation has ceased. During DM6, C_{inorg} Acc drops to a lower level.

18

Generally, mean C_{org} and C_{inorg} contents in the off-mound cores are on the same level, irrespective of the mound

505 formation phase. Regarding the on-mound cores, mean C_{org} content is slightly higher on BRI than on Dragon Mound, while C_{inorg} content is slightly higher on Dragon Mound. At a glance, all mean carbon content- and Acc values are higher for the CWC mounds, despite large variations in the off-mound cores.

5 Discussion

510 CWC mounds have been widely described as major carbonate factories (e.g., Titschack et al., 2009; 2015; 2016; Reimer et al., 2021) with elevated carbonate accumulation rates, and have been suggested as potentially important local to regional carbonate sinks. Previous accumulation studies, and broader estimates investigating CWC mounds off Norway, Ireland, Morocco, the Mediterranean Sea and off Namibia, found carbonate accumulation rates to be 2 – 11 times higher on the mounds compared to the adjacent seafloor or regional average (Lindberg and

515 Mienert, 2005; Dorschel et al., 2007b; Titschack et al., 2009, 2015, 2016; Hebbeln et al., 2019; Tamborrino et al., 2022). However, just two study have directly measured and compared carbonate accumulation on a mound to the immediate surrounding environment (Titschack et al., 2009, 2015), and all studies so far have focused on carbonate accumulation. This study provides a first holistic approach looking at the total carbon accumulation, including both C_{inorg} and C_{org} Acc on two mounds, and two nearby off-mound records. To make any conclusion about carbon

520 accumulation rates and whether the studied CWC mounds are effective carbon sinks, comparability is essential. Ultimately, this raises the unresolved question of what timeframes we should be looking at when discussing carbon sinks (Rossi and Rizzo 2020).

The comparability of accumulation rates between different ecosystems (also different CWC mound records) depends strongly on the considered time interval. The so-called "time-averaging effect" complicates comparisons

525 between records, with generally decreasing accumulation rates in correspondence to increasing time intervals analysed (e. g., Schlager, 2003). For instance, present-day shallow-water reefs are carbonate factories, which were locally absent during the glacial intervals due to sea-level fluctuations and thus, periodically swing between states of active formation and extinction (e. g., Schlager, 1981; Milliman, 1993; Wood et al., 2023). If carbon accumulation rates of such ecosystems are not only calculated for their active formation phase, but also include

530 periods of their temporal, local extinction, the time-averaging effects shifts the accumulation rates to lower values. This also relates to rates within formation phases if the accumulation rates show large variations as it is the case in CWC mound records. Hence, any comparison of (CWC mound) carbonate and carbon accumulation rates has to be done with utter caution, aware of whether these rates are calculated for large time-scales across several (CWC mound) formation phases interrupted by periods of extinction (e.g. Titschack et al. 2009; the latter partly covering

535 time intervals of hundreds of kyr), for intermediate time-scales treating each (CWC mound) formation phase separately (~tens of kyr; this study), or for individual "units" within one (CWC mound) formation phase (~hundreds of yr; e.g., Titschack et al. 2015). For instance, Norwegian CWC mound formation exhibits short-term maxima of up to >2000 g $CaCO_3$ cm^{-2} kyr^{-1} (Titschack et al., 2015). However, averaged across the entire mound formation phase record, aggradation- and accumulation rates off Norway are on the same level as the enhanced

540 mound formation phases described here (~100 g $CaCO_3$ cm^{-2} kyr^{-1}).

Thus, for consistency, we have chosen to look at complete mound formation phases, which are compared to the exact same period in the off-mound records. This approach allows the comparison of mound formation phases

discussed in this study with to total mean rates from Titschack et al. (2015; 2016), who calculated accumulation

rates over similar timespans (~3 – 8 kyr). Ultimately, only studies that analysed core records covering similar time

545   periods of at least >1 kyr were selected for further comparisons between CWC mound records or with other

ecosystems.

5.1 Patterns of Carbon(ate) Accumulation in CWC mounds across space and time

Based on the mean and min-max range in total carbon(ate) accumulation for each mound formation phase in our

550   study (Table 3), we identified the three different groups of accumulation: Phases of high carbon(ate) accumulation

(DM5, DM6, BRI$_{final}$; mean >100 g CaCO$_3$ cm^{-2} kyr^{-1} and ~15 g C cm^{-2} kyr^{-1}), phases of moderate carbon(ate)

accumulation (DM2, DM3; 49 – 53 g CaCO$_3$ cm^{-2} kyr^{-1} and 6 – 7 g C cm^{-2} kyr^{-1}), and phases of slow carbon(ate)

accumulation (DM1, DM4; <16 g CaCO$_3$ cm^{-2} kyr^{-1} and 1 – 2 g C cm^{-2} kyr^{-1}). These correspond each to high (>100

cm kyr^{-1}), moderate (<100 and >20 cm kyr^{-1}), and low (<20 cm kyr^{-1}) CWC mound ARs. A similar pattern has

555   also been found for CWC mounds studied by Titschack et al. (2015; 2016; Norway; Mediterranean). For instance,

compared to the high carbonate-accumulating mound formation phases in this study (AR ~140 cm kyr^{-1}; ~110 g

CaCO$_3$ cm^{-2} kyr^{-1}), the Norwegian CWC mounds of Træna Reef have very similar ARs (138 cm kyr^{-1}) and

accumulate a similar amount of carbonate, with 103 g CaCO$_3$ cm^{-2} kyr^{-1} during a comparable timespan (~4 kyr;

Titschack et al., 2015). Combining our new data with all mean values from Titschack et al. (2015; 2016), we find

560   an overall correlation of $R^2 = 0.91$ (p <0.0001) between ARs and on-mound carbonate accumulation rates for CWC

mounds (Fig. 5), suggesting that carbonate accumulation is mainly driven by ARs, and that the sediment
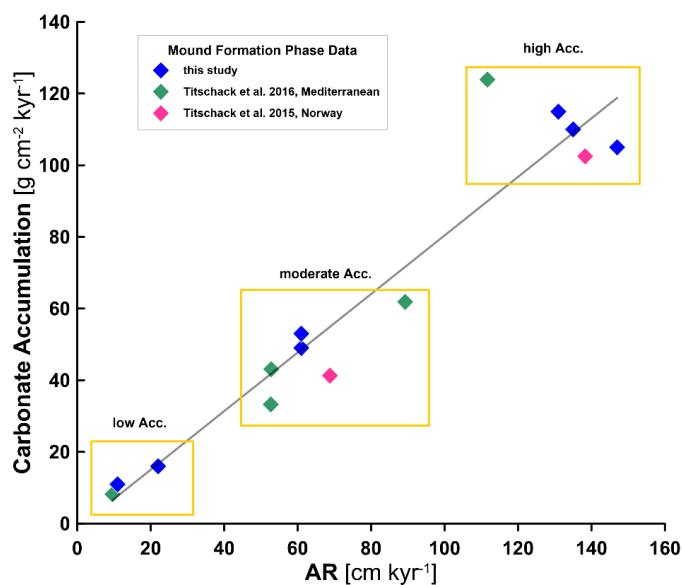
composition plays a subordinate role.

Fig. 5: Cross-plot outlining the relationship between CWC mound aggradation rates (AR) and carbonate accumulation

565   **rate with an R² = 0.91 (p <0.0001) for rates calculated for individual mound formation phases covering timespans of >2**

kyr (n= 14; blue symbols: this study, green symbols: Titschack et al.**, 2016 pink symbol: Titschack** et al.**, 2015).**

Enhanced mound formation phases with high ARs of >100 cm kyr^{-1}, as presented above, have been reported from many more CWC mound provinces (when averaged across similar timespans), such as Mauritania (Wienberg et

570 al., 2018; Wienberg et al., 2023), Namibia (Tamborrino et al., 2019) and Scotland (Douarin et al., 2013; Douarin et al., 2014). Based on the correlation we found (Fig. 5), we assume that these CWC mound provinces also accumulate high amounts of carbon(ate). Using a 70-m-long MeBo core record, we can for the first time compare carbon(ate) accumulation rates on the same CWC mound at the resolution of individual mound formation phases. This study shows that carbon(ate) accumulation occurred at comparable rates during young and old mound

575 formation phases, making a secondary loss of carbon by diagenetic processes unlikely, and confirms the potential for long-term carbon storage. In addition, the CWC mounds discovered to date are all located on passive continental margins (cf. Bradley, 2008), further highlighting their potential as very long-term carbon sinks.

5.2 The Role of Sediments in Carbon Accumulation on CWC Mounds

580 Our results demonstrate that sediments are not only essential for CWC mound formation (Thiem et al., 2006; Wheeler et al., 2007; Roberts et al., 2009; Pirlet et al., 2011; Wang et al., 2021), but also play a substantial role for carbon storage within the mounds with a contribution of up to 70 % (Table 3). During phases of enhanced CWC mound formation, i.e., high ARs, fast-growing coral frameworks are preserved in upright-position and provide accommodation space and baffling capacity for greater sediment deposition (Wang et al., 2021; see also Dorschel

585 et al., 2007a; Wheeler et al., 2008; Huvenne et al., 2009; Titschack et al., 2009, 2015). This results in mound deposits with low coral and high sediment contents. In contrast, slower-growing CWC frameworks get degraded over time, creating a coral rubble layer with less sediment baffling capacity, resulting in mound deposits with high coral and low sediment contents (Titschack et al., 2015; 2016; Wang et al., 2021). However, there are also other factors influencing the contribution of the sedimentary carbon fraction to the total carbon accumulation on a CWC

590 mound. While during the enhanced Dragon Mound formation phases (DM5; DM6), the sedimentary carbon fraction dominates the carbon accumulation (contributes 57 – 70 % to the total carbon accumulation; Table 3), the most recent mound formation phase documented for BRI (BRI$_{final}$) shows a relatively lower contribution of 48 % (Tables 2, 3) despite a comparable mound AR. This implies that, while carbon(ate) accumulation is steered by ARs, the overall contribution of sedimentary carbon to the total carbon accumulation on a mound can vary, when

595 averaging rates over entire mound formation phases. One explanation for this could be that BRI is located slightly deeper and further away from the coast compared to Dragon Mound: Naturally, the amount of sediment input increases with proximity to shore / nearest rivers mouths (e.g., Diesing, 2020; Epstein et al., 2024).

5.3 The Role of Organic Carbon in CWC Mounds: A Geological Perspective

600 For the first time, we demonstrate that also C$_{org}$ Acc on the studied CWC mounds is higher, compared to the adjacent off-mound deposits. This is partly due to a higher AR of CWC mound deposits. Independent of the AR, on-mound matrix sediments are selectively enriched in C$_{org}$, expressed as higher sediment C$_{org}$ wt.%, compared to the sediment of the adjacent seafloor (off-mound) by a factor of 1.2 – 1.4 (Table 4). This indicates that C$_{org}$ not only gets accumulated faster on the mounds, but that the material itself is enriched in C$_{org}$. Thus, CWC mounds

605   are effective sinks of C_{org} due to 1) the higher CWC mound ARs compared to sedimentation rates on the adjacent seafloor, and 2) selective enrichment in C_{org} of the mound matrix sediments.

While CWC mounds are generally located in areas of high bottom currents (Mienis et al., 2007; Dorschel et al., 2009; Hebbeln et al., 2016), the coral framework itself locally reduces the regional flow speed by up to 70%, changes the carrying capacity of the water mass, and allows the deposition of suspended, fine-grained and lighter
610   sediment particles between the corals (Bartzke et al., 2021; Wang et al. 2021). There is a link between fining of sediments and increase in C_{org} content (e. g., Dahl et al., 2016; Paradis et al., 2023), which has also been observed on CWC mounds (Kiriakoulakis et al., 2007; Stalder et al., 2018). This suggests that, despite strong bottom currents, C_{org}-rich sediment particles (large-surface area per weight, low density; Bergamaschi et al., 1997; Paradis et al., 2023) were trapped on the mound through the baffling effect of the coral framework (Wang et al., 2021;
615   Corbera et al., 2022), while at the same time, the adjacent (off-mound) seafloor faced a sediment bypass situation (*sensu* Wang et al., 2021). In addition, pycnocline-related nepheloid layers, carried by internal waves, certainly play a role in the transport of C_{org} across the Alborán Sea (Masqué et al., 2003; Puig et al., 2004; Sanchez-Vidal et al., 2005), and have been widely attributed to the occurrence of CWCs and mounds (Frederiksen et al., 1992; Mienis et al., 2007; Hanz et al., 2019). Following this concept, Wang et al. (2019) and Corbera et al. (2021) also
620   suggested internal waves as a key control on CWC reef development within the southern Alborán Sea, by delivering C_{org}-rich materials as food to the corals on CWC mounds in certain depth intervals. Ultimately, it is currently unclear whether the selective enrichment of C_{org} within the mound records is caused by nepholoid layer formation and/or a C_{org} bypass situation in the off-mound setting due to a lack of baffling capacity (absence of CWC framework). Large CWC mounds, forming significant elevations on the seafloor, can also self-induce local
625   downward transport of organic matter towards the mound summit (Mohn et al., 2014; Cyr et al., 2016; Soetart et al., 2016; van der Kaaden et al., 2021), which may further contribute to a higher C_{org} supply to mounds, compared to the plain seafloor.

Notably, it is the combination of (i) outlined physical hydrodynamic processes and (ii) biological processes that controls the C_{org} Acc on a CWC mound. Both processes happen at two scales: While at a larger hydrodynamic
630   scale, C_{org} is delivered to the reef by currents, the baffling of C_{org} happens at the scale of the coral frameworks on the mound. From a biological perspective, C_{org} is produced at a large scale by primary (C_{org}) production in the surface ocean, and after being supplied to the CWC mound, biological processes at the local scale of the reef further determine how much C_{org} eventually gets accumulated. Thriving CWC reefs are highly productive and considered hotspots of biomass, metabolism and C_{org} turnover (Oevelen et al., 2009; Cathalot et al., 2015; De
635   Clippele et al., 2021a; De Clippele et al., 2021b). This includes further recycling of organic waste products within the CWC reef's food web (Maier et al., 2020; 2023). As primary production-derived C_{org} is exclusively respired or transformed, but not newly produced by the heterotroph CWC reef fauna, C_{org} accumulation in CWC mound should be lower compared to off-mound deposits. Accordingly, high-level metabolism (i.e., higher carbon turnover relative to the surrounding seafloor; de Froe et al., 2019; De Clippele et al., 2021a) within the reef framework may
640   reduce the amount of C_{org} available for accumulation in the sediment (Wehrmann et al., 2009). This is in contrast to our finding that CWC mound sediment deposits are enriched in C_{org} and have higher C_{org} Acc rates compared to the off-mound deposits. Two studies on CWC reef surface sediments (North East Atlantic) also found a C_{org} wt.%-enriched top layer, relative to an off-mound setting (Kiriakoulakis et al., 2004; de Froe et al., 2019). Consequently, the sediments arriving at the CWC mound may initially have an even higher C_{org}-enrichment, but

645　the CWC reef fauna prevented part of it from being buried in the long-term. On the other hand, other benthic ecosystems characterised by high biodiversity and species density exhibit enhanced levels of C_{org}-rich detritus, bioturbation, etc. which may also increase the quantity of C_{org} buried (Canfield, 1994; Karlson et al., 2010; Strong et al., 2015; James et al., 2024). However, it is unknown what role these processes play on CWC reefs. This all emphasises that, especially regarding C_{org} burial, the complex interplay here on CWC mounds between biological

650　and geological processes with regards to C_{org} burial is poorly understood or quantified.

5.4 Cold-water coral mounds as carbon sinks

Carbon sinks are natural systems that remove carbon from the atmosphere, and store it in the bio-, hydro-, or lithosphere (Baker, 2007; Hiraishi et al., 2014; Howard et al., 2017). CWC mounds transfer carbon from the short-

655　term carbon cycle (atmosphere-hydrosphere) into the long-term carbon cycle (lithosphere). While the C_{inorg} sink removes dissolved inorganic carbon from the surrounding water mass, the C_{org} sink relies on C_{org} production in the surface ocean (primary production), hence removes carbon from the surface ocean. Consequently, both carbon sinks remove carbon from different short-term reservoirs.

Our study provides quantitative evidence that burial of both C_{inorg} and C_{org} happen at enhanced rates on CWC

660　mounds. More specifically, we found that during the same period, total carbon accumulation on two Mediterranean CWC mounds exceeds the rates from the adjacent seafloor by a factor of 14 – 19 during the same period. For C_{inorg} Acc (carbonate) individually, a factor of 15 – 19 results from our record, confirming that CWC mounds are effective local carbonate factories. As a novelty, this study highlights the additional importance of CWC mounds as long-term sinks for C_{org}. The accumulation of C_{org} is 9 –14 times higher on the CWC mounds, not only due to

665　the enhanced sediment deposition within coral mounds, but also due to a higher C_{org} content of the deposited sediment.

Here we present a ~400 kyr record of CWC mound formation in the Alborán Sea, but notably, there were extensive periods without any mound formation (see hiatuses, Fig. 3). Our comparison with the off-mound only covers the last ~115 kyrs, and earlier mound formation phases partly show much lower ARs / carbon accumulation rates.

670　However, despite the lack of mound formation (i.e., sedimentation) during the last 100 kyrs, Dragon Mound is still a topographic high, i.e., has not been buried, which demonstrates that the mounds overall accumulate more sediment and more carbon than the adjacent seafloor, also averaged across multiple interglacial-glacial cycles (see also Titschack et al., 2009). The total Holocene average C_{org} Acc for sediment drift deposits lies at 0.09 g C cm^{-2} kyr^{-1} (Yin et al., 2024), which matches perfectly with our mean C_{org} Acc from the off-mound records. This suggests

675　that our values are representative for hydrodynamic environments surrounding CWC mounds.

Amounting to a mean carbonate accumulation of 105 – 115 g CaCO$_3$ cm^{-2} kyr^{-1} during the last three enhanced mound formation phases, the studied mounds in the western Mediterranean Sea exhibit rates that are similar to tropical coral reefs (mean of ~120 g CaCO$_3$ cm^{-2} kyr^{-1}; Milliman, 1993). When looking at total carbon

680　accumulation, the studied CWC mounds accumulate ~ 1 – 15 g C cm^{-2} kyr^{-1} during phases of active mound formation, while in a global context, continental slopes are estimated to accumulate <0.2 g C cm^{-2} kyr^{-1} (Milliman, 1993). More specifically, other carbon storing-ecosystems like peatlands accumulate carbon at a rate of 1.4 – 2.2

23

g C cm^{-2} kyr^{-1} (Roulet et al., 2007), seagrass meadows ~3.6 g C cm^{-2} kyr^{-1} (Samper-Villarreal et al., 2018; export production not considered) and salt marshes ~4.0 g C cm^{-2} kyr^{-1} (Johnson et al., 2007). These examples outline

685   that CWC mounds can accumulate carbon at a similar rate as other, well-known carbon-storing ecosystems.

6 Conclusion

This study presents a first calculation of the total carbon accumulation, including inorganic (C$_{inorg}$) and organic carbon (C$_{org}$), on two CWC mounds in the western Mediterranean (Alborán Sea) showing that active CWC mounds

690   can be effective carbon sinks across geological timescales. During times of enhanced mound formation with mound ARs of >100 cm kyr^{-1}, the total carbon accumulation lies at ~15 g C cm^{-2} kyr^{-1}, and is estimated to be 14 – 19 times higher than in the adjacent seafloor deposits during the same time period. We highlight that CWC mounds effectively act as local carbon sinks for both C$_{inorg}$ and C$_{org}$ during mound formation phases. Moreover, CWC mounds accumulate carbon at a similar level as other ecosystems, e. g., salt marshes, sea grass meadows or

695   peatlands, that are known for their high carbon-storing capacity. We find that high carbonate accumulation rates correlate with high mound ARs. With multiple known CWC mound provinces exhibiting high ARs of >100 cm kyr^{-1}, we speculate that CWC mounds may play a vital role in the carbon budget of many regions. However, more studies on the role of CWC mounds in the long-term carbon cycle and on the dynamics of carbon accumulation across time and space are needed to validate this. Knowledge about the distribution and abundance of CWC

700   mounds along the world's continental margins is still very limited, which currently hinders further upscaling.

We underline with our data that the contribution of sedimentary carbon is crucial in the process of on-mound carbon accumulation. Furthermore, sediment-derived C$_{org}$ may play a previously overlooked, important role in on-mound carbon accumulation, and our data suggest that CWC mound sediments may be selectively enriched in C$_{org}$. C$_{org}$ contributes 6 – 9 % to total carbon accumulation on the studied CWC mounds, and needs to be considered

705   when evaluating carbon accumulation of marine carbonate factories.

Through analysing a total timespan of ~400 kyr and investigating all major compartments of carbon accumulation, this study provides a step towards including CWC mounds into global marine carbon budget assessments. On that note, an increasing number of studies highlight the overlooked role that marine fauna and heterotroph ecosystems as a whole play in transferring carbon between different carbon reservoirs (i.e., atmosphere, hydrosphere,

710   biosphere and litosphere; Schmitz et al., 2014; Schmitz et al., 2018; James et al., 2024).

Data Availability

All unpublished raw data are made available through the open access data repository and World Data Center PANGAEA.

715

Author Contributions

DH conceptualised the study, JT and LG designed the methodology. DH and CW organized the data collection and conducted the field work. JT and LG performed the Computed Tomography measurements. HW contributed

further data sets to the study. LG conducted the formal analysis wrote the original draft, and all authors were
720 involved in the interpretation of the results, the revision and the writing of the final version of the manuscript.

Competing Interests

The authors declare that they have no conflict of interest.

References

740

Álvarez, M., Catalá, T. S., Civitarese, G., Coppola, L., Hassoun, A. E. R., Ibello, V., Lazzari, P., Lefevre, D.,
Macías, D., Santinelli, C., and Ulses, C.: Mediterranean Sea general biogeochemistry, in: Oceanography of the
Mediterranean Sea, edited by: Schroeder, K. and Chiggiato, J., Elsevier, 387–451, https://doi.org/10.1016/B978-
0-12-823692-5.00004-2, 2023.

745 Baker, D. F.: Reassessing Carbon Sinks, *Science*, 317, 1708–1709, https://doi.org/10.1126/science.1144863,
2007.

Bartzke, G., Siemann, L., Büssing, R., Nardone, P., Koll, K., Hebbeln, D., and Huhn, K.: Investigating the
Prevailing Hydrodynamics Around a Cold-Water Coral Colony Using a Physical and a Numerical Approach,
Front. Mar. Sci., 8, https://doi.org/10.3389/fmars.2021.663304, 2021.

750 Bergamaschi, B. A., Tsamakis, E., Keil, R. G., Eglinton, T. I., Montluçon, D. B., and Hedges, J. I.: The effect of
grain size and surface area on organic matter, lignin and carbohydrate concentration, and molecular
compositions in Peru Margin sediments, *Geochim. Cosmochim. Ac.*, 61, 1247–1260,
https://doi.org/10.1016/S0016-7037(96)00394-8, 1997.

Blum, P.: Physical Properties Handbook: A Guide to the Shipboard Measurement of Physical Properties of
755 Deep-Sea Cores, College Station, Texas, USA, http://www-odp.tamu.edu, 1997.

Bradley, D. C.: Passive margins through earth history, *Earth-Sci. Rev.*, 91, 1–26, https://doi.org/10.1016/j.earscirev.2008.08.001, 2008.

Burdige, D. J.: Preservation of Organic Matter in Marine Sediments: Controls, Mechanisms, and an Imbalance in Sediment Organic Carbon Budgets?, *Chem. Rev.*, 107, 467–485, https://doi.org/10.1021/cr050347q, 2007.

760 Butzin, M., Köhler, P., and Lohmann, G.: Marine radiocarbon reservoir age simulations for the past 50,000 years, *Geophys. Res. Lett.*, 44, 8473–8480, https://doi.org/10.1002/2017gl074688, 2017.

Canfield, D. E.: Factors influencing organic carbon preservation in marine sediments, *Chem. Geol.*, 114, 315–329, https://doi.org/10.1016/0009-2541(94)90061-2, 1994.

Cartapanis, O., Galbraith, E. D., Bianchi, D., and Jaccard, S. L.: Carbon burial in deep-sea sediment and
765 implications for oceanic inventories of carbon and alkalinity over the last glacial cycle, *Clim. Past*, 14, 1819–1850, https://doi.org/10.5194/cp-14-1819-2018, 2018.

Cathalot, C., Van Oevelen, D., Cox, T. J. S., Kutti, T., Lavaleye, M., Duineveld, G., and Meysman, F. J. R.: Cold-water coral reefs and adjacent sponge grounds: hotspots of benthic respiration and organic carbon cycling in the deep sea, *Front. Mar. Sci.*, 2, https://doi.org/10.3389/fmars.2015.00037, 2015.

770 Corbera, G., Lo Iacono, C., Gràcia, E., Grinyó, J., Pierdomenico, M., Huvenne, V. A. I., Aguilar, R., and Gili, J. M.: Ecological characterisation of a Mediterranean cold-water coral reef: Cabliers Coral Mound Province (Alboran Sea, western Mediterranean), *Prog. Oceanogr.*, 175, 245–262, https://doi.org/10.1016/j.pocean.2019.04.010, 2019.

Corbera, G., Lo Iacono, C., Simarro, G., Grinyó, J., Ambroso, S., Huvenne, V. A. I., Mienis, F., Carreiro-Silva,
775 M., Martins, I., Mano, B., Orejas, C., Larsson, A., Hennige, S., and Gori, A.: Local-scale feedbacks influencing cold-water coral growth and subsequent reef formation, *Sci. Rep.*, 12, 20389, https://doi.org/10.1038/s41598-022-24711-7, 2022.

Corbera, G., Lo Iacono, C., Standish, C. D., Anagnostou, E., Titschack, J., Katsamenis, O., Cacho, I., Van Rooij, D., Huvenne, V. A. I., and Foster, G. L.: Glacio-eustatic variations and sapropel events as main controls on the
780 Middle Pleistocene-Holocene evolution of the Cabliers Coral Mound Province (W Mediterranean), *Quat. Sci. Rev.*, 253, https://doi.org/10.1016/j.quascirev.2020.106783, 2021.

Cyr, F., van Haren, H., Mienis, F., Duineveld, G., and Bourgault, D.: On the influence of cold-water coral mound size on flow hydrodynamics, and vice versa, *Geophys. Res. Lett.*, 43, 775–783, https://doi.org/10.1002/2015GL067038, 2016.

785 Dahl, M., Deyanova, D., Gutschow, S., Asplund, M. E., Lyimo, L. D., Karamfilov, V., Santos, R., Bjork, M., and Gullstrom, M.: Sediment Properties as Important Predictors of Carbon Storage in Zostera marina Meadows: A Comparison of Four European Areas, *PLoS One*, 11, e0167493, https://doi.org/10.1371/journal.pone.0167493, 2016.

De Clippele, L. H., Rovelli, L., Ramiro-Sánchez, B., Kazanidis, G., Vad, J., Turner, S., Glud, R. N., and Roberts,
790 J. M.: Mapping cold-water coral biomass: an approach to derive ecosystem functions, *Coral Reefs*, 40, 215–231, https://doi.org/10.1007/s00338-020-02030-5, 2021a.

De Clippele, L. H., van der Kaaden, A.-S., Maier, S. R., de Froe, E., and Roberts, J. M.: Biomass Mapping for an Improved Understanding of the Contribution of Cold-Water Coral Carbonate Mounds to C and N Cycling, *Front. Mar. Sci.*, 8, https://doi.org/10.3389/fmars.2021.721062, 2021b.

795 de Froe, E., Rovelli, L., Glud, R. N., Maier, S. R., Duineveld, G., Mienis, F., Lavaleye, M., and van Oevelen, D.: Benthic Oxygen and Nitrogen Exchange on a Cold-Water Coral Reef in the North-East Atlantic Ocean, *Front. Mar. Sci.*, 6, https://doi.org/10.3389/fmars.2019.00665, 2019.

de Haas, H., Mienis, F., Frank, N., Richter, T. O., Steinacher, R., de Stigter, H., van der Land, C., and van Weering, T. C. E.: Morphology and sedimentology of (clustered) cold-water coral mounds at the south Rockall

800   Trough margins, NE Atlantic Ocean, *Facies*, 55(1), 1–26, https://doi.org/10.1007/s10347-008-0157-1, 2009.

Diesing, M.: Deep-sea sediments of the global ocean, *Earth Syst. Sci. Data*, 12(4), 3367–3381, https://doi.org/10.5194/essd-12-3367-2020, 2020.

Dorschel, B., Hebbeln, D., Foubert, A., White, M., and Wheeler, A. J.: Hydrodynamics and cold-water coral facies distribution related to recent sedimentary processes at Galway Mound west of Ireland, *Mar. Geol.*, 244(1–

805   4), 184–195, https://doi.org/10.1016/j.margeo.2007.06.010, 2007a.

Dorschel, B., Hebbeln, D., Rüggeberg, A., and Dullo, C.: Carbonate budget of a cold-water coral carbonate mound: Propeller Mound, Porcupine Seabight, *Int. J. Earth Sci.*, 96(1), 73–83, https://doi.org/10.1007/s00531-005-0493-0, 2007b.

Dorschel, B., Hebbeln, D., Rüggeberg, A., Dullo, W., and Freiwald, A.: Growth and erosion of a cold-water

810   coral covered carbonate mound in the Northeast Atlantic during the Late Pleistocene and Holocene, *Earth Planet. Sci. Lett.*, 233(1–2), 33–44, https://doi.org/10.1016/j.epsl.2005.01.035, 2005.

Dorschel, B., Wheeler, A. J., Huvenne, V. A. I., and de Haas, H.: Cold-water coral mounds in an erosive environmental setting: TOBI side-scan sonar data and ROV video footage from the northwest Porcupine Bank, NE Atlantic, *Mar. Geol.*, 264(3–4), 218–229, https://doi.org/10.1016/j.margeo.2009.06.005, 2009.

815   Douarin, M., Elliot, M., Noble, S. R., Sinclair, D., Henry, L.-A., Long, D., Moreton, S. G., and Roberts, J. M.: Growth of north-east Atlantic cold-water coral reefs and mounds during the Holocene: A high resolution U-series and 14C chronology, *Earth Planet. Sci. Lett.*, 375, 176–187, https://doi.org/10.1016/j.epsl.2013.05.023, 2013.

Douarin, M., Sinclair, D. J., Elliot, M., Henry, L.-A., Long, D., Mitchison, F., and Roberts, J. M.: Changes in

820   fossil assemblage in sediment cores from Mingulay Reef Complex (NE Atlantic): Implications for coral reef build-up, *Deep Sea Res. Pt. II: Top. Stud. Oceanogr.*, 99, 286–296, https://doi.org/10.1016/j.dsr2.2013.07.022, 2014.

Duchesne, M. J., Moore, F., Long, B. F., and Labrie, J.: A rapid method for converting medical Computed Tomography scanner topogram attenuation scale to Hounsfield Unit scale and to obtain relative density values,

825   *Eng. Geol.*, 103(3–4), 100–105, https://doi.org/10.1016/j.enggeo.2008.06.009, 2009.

Ercilla, G., Juan, C., Hernandez-Molina, F. J., Bruno, M., Estrada, F., Alonso, B., Casas, D., Farran, M. L., Llave, E., García, M., Vázquez, J. T., D'Acremont, E., Gorini, C., Palomino, D., Valencia, J., El Moumni, B., and Ammar, A.: Significance of bottom currents in deep-sea morphodynamics: an example from the Alboran Sea, *Mar. Geol.*, 378, 157–170, https://doi.org/10.1016/j.margeo.2015.09.007, 2016.

830   EMODnet   Bathymetry   Consortium: EMODnet   Digital   Bathymetry   (DTM   2022), https://doi.org/10.12770/ff3aff8a-cff1-44a3-a2c8-1910bf109f85, 2022. [DATASET]

Epstein, G., Fuller, S. D., Hingmire, D., Myers, P. G., Peña, A., Pennelly, C., and Baum, J. K.: Predictive mapping of organic carbon stocks in surficial sediments of the Canadian continental margin, *Earth Syst. Sci. Data*, 16, 2165–2195, https://doi.org/10.5194/essd-16-2165-2024, 2024.

835   Fentimen, R., Feenstra, E., Rüggeberg, A., Hall, E., Rime, V., Vennemann, T., Hajdas, I., Rosso, A., Van Rooij, D., Adatte, T., Vogel, H., Frank, N., and Foubert, A.: A 300 000-year record of cold-water coral mound build-up at the East Melilla Coral Province (SE Alboran Sea, western Mediterranean), *Clim. Past*, 18, 1915–1945, https://doi.org/10.5194/cp-18-1915-2022, 2022.

Fentimen, R., Feenstra, E., Rüggeberg, A., Vennemann, T., Hajdas, I., Adatte, T., Van Rooij, D., and Foubert,

840   A.: Cold-Water Coral Mound Archive Provides Unique Insights Into Intermediate Water Mass Dynamics in the Alboran Sea During the Last Deglaciation, *Front. Mar. Sci.*, 7, https://doi.org/10.3389/fmars.2020.00354, 2020.

Fentimen, R., Feenstra, E. J., Rüggeberg, A., Hall, E., Rosso, A., Hajdas, I., Jaramillo-Vogel, D., Grobéty, B., Adatte, T., Van Rooij, D., Frank, N., and Foubert, A.: Staggered cold-water coral mound build-up on an Alboran ridge during the last deglacial (East Melilla Mound Field, western Mediterranean), *Mar. Geol.*, 457,
845   https://doi.org/10.1016/j.margeo.2023.106994, 2023.

Fink, H. G., Wienberg, C., De Pol-Holz, R., Wintersteller, P., and Hebbeln, D.: Cold-water coral growth in the Alboran Sea related to high productivity during the Late Pleistocene and Holocene, *Marine Geology*, 339, 71–82, https://doi.org/10.1016/j.margeo.2013.04.009, 2013.

Frank, N., Ricard, E., Lutringer-Paquet, A., van der Land, C., Colin, C., Blamart, D., Foubert, A., Van Rooij, D.,
850   Henriet, J.-P., de Haas, H., and van Weering, T.: The Holocene occurrence of cold-water corals in the NE Atlantic: Implications for coral carbonate mound evolution, *Marine Geology*, 266, 129–142, https://doi.org/10.1016/j.margeo.2009.08.007, 2009.

Frederiksen, R., Jensen, A., and Westerberg, H.: The distribution of the scleractinian coral Lophelia pertusa around the Faroe Islands and the relation to internal tidal mixing, *Sarsia*, 77(2), 157–171,
855   https://doi.org/10.1080/00364827.1992.10413502, 1992.

Freudenthal, T., and Wefer, G.: Drilling cores on the sea floor with the remote-controlled sea floor drilling rig MeBo, *Geoscientific Instrumentation, Methods and Data Systems*, 2(2), 329–337, https://doi.org/10.5194/gi-2-329-2013, 2013.

GEBCO Compilation Group: GEBCO 2024 Grid, https://doi.org/10.5285/1c44ce99-0a0d-5f4f-e063-
860   7086abc0ea0f, 2024. [DATASET]

Gerland, S., and Villinger, H.: Nondestructive density determination on marine sediment cores from gamma-ray attenuation measurements, *Geo-Marine Letters*, 15, 111–118, https://doi.org/10.1007/BF01275415, 1995.

Hanz, U., Wienberg, C., Hebbeln, D., Duineveld, G., Lavaleye, M., Juva, K., Dullo, W.-C., Freiwald, A., Tamborrino, L., Reichart, G.-J., Flögel, S., and Mienis, F.: Environmental factors influencing benthic
865   communities in the oxygen minimum zones on the Angolan and Namibian margins, *Biogeosciences*, 16(22), 4337–4356, https://doi.org/10.5194/bg-16-4337-2019, 2019.

Hayes, D. R., Schroeder, K., Poulain, P.-M., Testor, P., Mortier, L., Bosse, A., and du Madron, X.: Review of the Circulation and Characteristics of Intermediate Water Masses of the Mediterranean: Implications for Cold-Water Coral Habitats, In: *Mediterranean Cold-Water Corals: Past, Present and Future Coral Reefs of the*
870   *World*, 195–211, https://doi.org/10.1007/978-3-319-91608-8_18, 2019.

Hebbeln, D.: Highly Variable Submarine Landscapes in the Alborán Sea Created by Cold-Water Corals. In: Orejas, C. and Jimenéz, C. (eds.), *Mediterr. Cold-Water Corals: Past, Present and Future*, Vol. 9, Coral Reefs of the World. https://doi.org/10.1007/978-3-319-91608-8_8, 2019.

Hebbeln, D., Bender, M., Gaide, S., Titschack, J., Vandorpe, T., Van Rooij, D., Wintersteller, P. and Wienberg,
875   C.: Thousands of cold-water coral mounds along the Moroccan Atlantic continental margin: Distribution and morphometry. *Mar. Geol.*, 411, 51–61. https://doi.org/10.1016/j.margeo.2019.02.001, 2019.

Hebbeln, D., Van Rooij, D. and Wienberg, C.: Good neighbours shaped by vigorous currents: Cold-water coral mounds and contourites in the North Atlantic. *Mar. Geol.*, 378, 171–185. https://doi.org/10.1016/j.margeo.2016.01.014, 2016.

880   Hebbeln, D., Wienberg, C., Bartels, M., Bergenthal, M., Frank, N., Gaide, S., Henriet, J. P., Kaszemeik, K., Klar, S., Klein, T., Krengel, T., Kuhnert, M., Meyer-Schack, B., Noorlander, C., Reuter, M., Rosiak, U., Schmidt, W., Seeba, H., Seiter, C., Strange, N., Terhzaz, L. and Van Rooij, D.: MoccoMeBo: Climate-driven development of Moroccan cold-water coral mounds revealed by MeBo-drilling: Atlantic vs. Mediterranean settings. https://doi.org/10.2312/cr_msm36, 2015.

885   Hebbeln, D., Wienberg, C., Beuck, L., Freiwald, A., Wintersteller, P. and cruise participants: Report and preliminary results of RV POSEIDON Cruise POS 385 "Cold-Water Corals of the Alboran Sea (western

Mediterranean Sea)", Faro - Toulon, May 29 - June 16, 2009., Bremen, Germany. http://nbn-resolving.de/urn:nbn:de:gbv:46-ep000106508, 2009.

890 Henry, L.-A. and Roberts, J. M.: Global biodiversity in cold-water coral reef ecosystems. In: Rossi, S., Bramanti, L., Gori, A. and Orejas, C. (eds.), *Marine Animal Forests*, Springer, 235–256. https://doi.org/10.1007/978-3-319-21012-4_6, 2017.

Hiraishi, T., Krug, T. and Tanabe, K.: Supplement to the 2006 IPCC guidelines for national greenhouse gas inventories: wetlands. Geneva, Switzerland, 2014.

Howard, J., Sutton-Grier, A., Herr, D., Kleypas, J., Landis, E., McLeod, E., Pidgeon, E. and Simpson, S.:
895 Clarifying the role of coastal and marine systems in climate mitigation. *Front. Ecol. Environ.*, 15(1), 42–50. https://doi.org/10.1002/fee.1451, 2017.

Huvenne, V. A. I., Van Rooij, D., De Mol, B., Thierens, M., O'Donnell, R. and Foubert, A.: Sediment dynamics and palaeo-environmental context at key stages in the Challenger cold-water coral mound formation: Clues from sediment deposits at the mound base. *Deep-Sea Res. I*, 56(12), 2263–2280.
900 https://doi.org/10.1016/j.dsr.2009.08.003, 2009.

IODP: Depth Scales Terminology, Ver. 2.0. https://www.iodp.org/policies-and-guidelines/142-iodp-depth-scales-terminology-april-2011/file, 2011.

James, K., Macreadie, P. I., Burdett, H. L., Davies, I. and Kamenos, N. A.: It's time to broaden what we consider a 'blue carbon ecosystem'. *Global Change Biol.*, 30(5), e17261. https://doi.org/10.1111/gcb.17261, 2024.

905 Johnson, B. J., Moore, K. A., Lehmann, C., Bohlen, C. and Brown, T. A.: Middle to late Holocene fluctuations of C3 and C4 vegetation in a Northern New England Salt Marsh, Sprague Marsh, Phippsburg Maine. *Org. Geochem.*, 38(3), 394–403. https://doi.org/10.1016/j.orggeochem.2006.06.006, 2007.

van der Kaaden, A., Mohn, C., Gerkema, T., Maier, S. R., de Froe, E., van de Koppel, J., Rietkerk, M., Soetaert, K. and van Oevelen, D.: Feedbacks between hydrodynamics and cold-water coral mound development. *Deep-*
910 *Sea Res. I*, 178, 103641. https://doi.org/10.1016/j.dsr.2021.103641, 2021.

Karlson, A. M., Nascimento, F. J., Naslund, J. and Elmgren, R.: Higher diversity of deposit-feeding macrofauna enhances phytodetritus processing. *Ecology*, 91(5), 1414–1423. https://doi.org/10.1890/09-0660.1, 2010.

Kiriakoulakis, K., Bett, B. J., White, M. and Wolff, G. A.: Organic biogeochemistry of the Darwin Mounds, a deep-water coral ecosystem, of the NE Atlantic. *Deep-Sea Res. I*, 51(12), 1937–1954.
915 https://doi.org/10.1016/j.dsr.2004.07.010, 2004.

Kiriakoulakis, K., Freiwald, A., Fisher, E. and Wolff, G. A.: Organic matter quality and supply to deep-water coral/mound systems of the NW European Continental Margin. *Int. J. Earth Sci.*, 96(1), 159–170. https://doi.org/10.1007/s00531-006-0078-6, 2007.

Korpanty, C. A., Hoffman, L., Portilho-Ramos, R. d. C., Titschack, J., Wienberg, C. and Hebbeln, D.: Decline in
920 cold-water coral growth promotes molluscan diversity: A paleontological perspective from a cold-water coral mound in the western Mediterranean Sea. *Front. Mar. Sci.*, 9. https://doi.org/10.3389/fmars.2022.895946, 2023.

Langner, M. and Mulitza, S.: Technical note: PaleoDataView – a software toolbox for the collection, homogenization and visualization of marine proxy data. *Climate Past*, 15(6), 2067–2072. https://doi.org/10.5194/cp-15-2067-2019, 2019.

925 Lindberg, B. and Mienert, J.: Postglacial carbonate production by cold-water corals on the Norwegian Shelf and their role in the global carbonate budget. *Geology*, 33(7). https://doi.org/10.1130/g21577.1, 2005.

Lisiecki, L. E. and Raymo, M. E.: A Pliocene-Pleistocene stack of 57 globally distributed benthic δ18O records. *Paleoceanography*, 20(1). https://doi.org/10.1029/2004pa001071, 2005.

930 Lo Iacono, C., Gràcia, E., Bartolomé, R., Comas, M. C., Dañobeitia, J. J. and Team, a. E.-S.: Acoustic imaging of carbonate mounds in the Chella Bank (Eastern Alboran Sea - SW Mediterranean). *Geo-Mar. Res. Med. Eur.-Atl. Marg.*, 2-5 February 2009, IOC Workshop Report No. 220, Granada, Spain: UNESCO, 52. https://unesdoc.unesco.org/ark:/48223/pf0000181342, 2009.

935 Lo Iacono, C., Gràcia, E., Ranero, C. R., Emelianov, M., Huvenne, V. A. I., Bartolomé, R., Booth-Rea, G., Prades, J., Ambroso, S., Dominguez, C., Grinyó, J., Rubio, E. and Torrent, J.: The West Melilla cold water coral mounds, Eastern Alboran Sea: Morphological characterization and environmental context. *Deep-Sea Res. II*, 99, 316–326. https://doi.org/10.1016/j.dsr2.2013.07.006, 2014.

Lougheed, B. C. and Obrochta, S. P.: A Rapid, Deterministic Age-Depth Modeling Routine for Geological Sequences With Inherent Depth Uncertainty. *Paleoceanogr. Paleoclimatol.*, 34(1), 122–133. https://doi.org/10.1029/2018pa003457, 2019.

940 Maier, S. R., Kutti, T., Bannister, R. J., Fang, J. K., van Breugel, P., van Rijswijk, P. and van Oevelen, D.: Recycling pathways in cold-water coral reefs: Use of dissolved organic matter and bacteria by key suspension feeding taxa. *Sci. Rep.*, 10(1), 9942. https://doi.org/10.1038/s41598-020-66463-2, 2020.

Maier, S. R., Brooke, S., De Clippele, L. H., de Froe, E., van der Kaaden, A.-S., Kutti, T., Mienis, F., and van Oevelen, D.: On the paradox of thriving cold-water coral reefs in the food-limited deep sea, *Biol. Rev.*, 98, 1298–
945 1316, https://doi.org/10.1111/brv.12976, 2023.

Margreth, S., Gennari, G., Rüggeberg, A., Comas, M. C., Pinheiro, L. M., and Spezzaferri, S.: Growth and demise of cold-water coral ecosystems on mud volcanoes in the West Alboran Sea: The messages from the planktonic and benthic foraminifera, *Mar. Geol.*, 282, 26–39, https://doi.org/10.1016/j.margeo.2011.02.006, 2011.

950 Masqué, P., Fabres, J., Canals, M., Sanchez-Cabeza, J. A., Sanchez-Vidal, A., Cacho, I., Calafat, A. M., and Bruach, J. M.: Accumulation rates of major constituents of hemipelagic sediments in the deep Alboran Sea: a centennial perspective of sedimentary dynamics, *Mar. Geol.*, 193, 207–233, https://doi.org/10.1016/S0025-3227(02)00593-5, 2003.

Michel, J., Laugié, M., Pohl, A., Lanteaume, C., Masse, J.-P., Donnadieu, Y., and Borgomano, J.: Marine
955 carbonate factories: a global model of carbonate platform distribution, *Int. J. Earth Sci.*, 108, 1773–1792, https://doi.org/10.1007/s00531-019-01742-6, 2019.

Mienis, F., de Stigter, H. C., White, M., Duineveld, G., de Haas, H., and van Weering, T. C. E.: Hydrodynamic controls on cold-water coral growth and carbonate-mound development at the SW and SE Rockall Trough Margin, NE Atlantic Ocean, *Deep-Sea Res. I*, 54, 1655–1674, https://doi.org/10.1016/j.dsr.2007.05.013, 2007.

960 Milliman, J. D.: Precipitation and Cementation of Deep-Sea Carbonate Sediments, in Inderbitzen, A. L. (ed.), *Deep-Sea Sediments: Physical and Mechanical Properties*, Springer US, Boston, MA, 463–476, https://doi.org/10.1007/978-1-4684-2754-7_23, 1974.

Milliman, J. D.: Production and accumulation of calcium carbonate in the ocean: Budget of a nonsteady state, *Global Biogeochem. Cycles*, 7, 927–957, https://doi.org/10.1029/93GB02524, 1993.

965 Millot, C.: Circulation in the western Mediterranean Sea, *J. Mar. Syst.*, 20, 423–442, https://doi.org/10.1016/S0924-7963(98)00078-5, 1999.

Mohn, C., Rengstorf, A., White, M., Duineveld, G., Mienis, F., Soetaert, K., and Grehan, A.: Linking benthic hydrodynamics and cold-water coral occurrences: A high-resolution model study at three cold-water coral provinces in the NE Atlantic, *Prog. Oceanogr.*, 122, 92–104, https://doi.org/10.1016/j.pocean.2013.12.003,
970 2014.

Morán, X. A. G., and Estrada, M.: Short-term variability of photosynthetic parameters and particulate and dissolved primary production in the Alboran Sea (SW Mediterranean), *Mar. Ecol. Prog. Ser.*, 212, 53–67, https://doi.org/10.3354/meps212053, 2001.

O'Mara, N. A., and Dunne, J. P.: Hot Spots of Carbon and Alkalinity Cycling in the Coastal Oceans, *Sci. Rep.*, 9,
975 4434, https://doi.org/10.1038/s41598-019-41064-w, 2019.

van Oevelen, D., Duineveld, G., Lavaleye, M., Mienis, F., Soetaert, K., and Heip, C. H. R.: The cold-water coral
community as hotspot of carbon cycling on continental margins: A food-web analysis from Rockall Bank
(northeast Atlantic), *Limnol. Oceanogr.*, 54, 1829–1844, https://doi.org/10.4319/lo.2009.54.6.1829, 2009.

Orsi, T. H., and Anderson, A. L.: Bulk density calibration for X-ray tomographic analyses of marine sediments,
980 *Geo-Mar. Lett.*, 19, 270–274, https://doi.org/10.1007/s003670050118, 1999.

Orsi, T. H., Edwards, C. M., and Anderson, A. L.: X-ray computed tomography: a nondestructive method for
quantitative analysis of sediment cores, *J. Sediment. Res.*, 64, 3, https://doi.org/10.1306/D4267E74-2B26-11D7-
8648000102C1865D, 1994.

Paradis, S., Nakajima, K., Van der Voort, T. S., Gies, H., Wildberger, A., Blattmann, T. M., Bröder, L., and
985 Eglinton, T. I.: The Modern Ocean Sediment Archive and Inventory of Carbon (MOSAIC): version 2.0, *Earth
Syst. Sci. Data*, 15, 4105–4125, https://doi.org/10.5194/essd-15-4105-2023, 2023.

Pirlet, H., Colin, C., Thierens, M., Latruwe, K., Van Rooij, D., Foubert, A., Frank, N., Blamart, D., Huvenne, V.
A. I., Swennen, R., Vanhaecke, F., and Henriet, J.-P.: The importance of the terrigenous fraction within a cold-
water coral mound: A case study, *Mar. Geol.*, 282, 13–25, https://doi.org/10.1016/j.margeo.2010.05.008, 2011.

990 Puig, P., Palanques, A., Guillén, J., and El Khatab, M.: Role of internal waves in the generation of nepheloid
layers on the northwestern Alboran slope: Implications for continental margin shaping, *J. Geophys. Res.:
Oceans*, 109, C9, https://doi.org/10.1029/2004jc002394, 2004.

Reijmer, J. J. G.: Marine carbonate factories: Review and update, *Sedimentology*, 68, 1729–1796,
https://doi.org/10.1111/sed.12878, 2021.

995 Reimer, P. J., Austin, W. E. N., Bard, E., Bayliss, A., Blackwell, P. G., Bronk Ramsey, C., Butzin, M., Cheng,
H., Edwards, R. L., Friedrich, M., Grootes, P. M., Guilderson, T. P., Hajdas, I., Heaton, T. J., Hogg, A. G.,
Hughen, K. A., Kromer, B., Manning, S. W., Muscheler, R., Palmer, J. G., Pearson, C., van der Plicht, J.,
Reimer, R. W., Richards, D. A., Scott, E. M., Southon, J. R., Turney, C. S. M., Wacker, L., Adolphi, F.,
Büntgen, U., Capano, M., Fahrni, S. M., Fogtmann-Schulz, A., Friedrich, R., Köhler, P., Kudsk, S., Miyake, F.,
1000 Olsen, J., Reinig, F., Sakamoto, M., Sookdeo, A., and Talamo, S.: The IntCal20 Northern Hemisphere
Radiocarbon Age Calibration Curve (0–55 cal kBP), *Radiocarbon*, 62, 725–757,
https://doi.org/10.1017/rdc.2020.41, 2020.

Ridgwell, A., and Zeebe, R.: The role of the global carbonate cycle in the regulation and evolution of the Earth
system, *Earth Planet. Sci. Lett.*, 234, 299–315, https://doi.org/10.1016/j.epsl.2005.03.006, 2005.

1005 Roberts, J. M., Freiwald, A., Wheeler, A., and Cairns, S.: Cold-Water Corals, *Cambridge Univ. Press*,
https://doi.org/10.1017/cbo9780511581588.005, 2009.

Roberts, J. M., Wheeler, A. J., and Freiwald, A.: Reefs of the Deep: The Biology and Geology of Cold-Water
Coral Ecosystems, *Science*, 312, 543–547, https://doi.org/10.1126/science.1119861, 2006.

Van Rooij, D., Hebbeln, D., Comas, M. C., Vandorpe, T., Delivet, S., and Scientists, M. S.: EUROFLEETS
1010 Cruise Summary Report GATEWAY. The Mediterranean-Atlantic Gateway Code: The Late Pleistocene
Carbonate Mound Record. R/V Marion Dufresne, Cruise No. 194, 10–20 June 2013, Cadiz (Spain) - Lisbon
(Portugal), https://doi.org/10.17600/13200130, 2013.

Rossi, S., and Rizzo, L.: Marine Animal Forests as Carbon Immobilizers or Why We Should Preserve These
Three-Dimensional Alive Structures, in Rossi, S. and Bramanti, L. (eds.), *Perspect. Mar. Anim. Forests World*,
1015 333–400, https://doi.org/10.1007/978-3-030-57054-5_11, 2020.

Roulet, N. T., Lafleur, P. M., Richard, P. J. H., Moore, T. R., Humphreys, E. R., and Bubier, J.: Contemporary carbon balance and late Holocene carbon accumulation in a northern peatland, *Global Change Biol.*, 13, 397–411, https://doi.org/10.1111/j.1365-2486.2006.01292.x, 2007.

1020 Samper-Villarreal, J., Mumby, P. J., Saunders, M. I., Barry, L. A., Zawadzki, A., Heijnis, H., Morelli, G., and Lovelock, C. E.: Vertical accretion and carbon burial rates in subtropical seagrass meadows increased following anthropogenic pressure from European colonisation, *Estuar. Coast. Shelf Sci.*, 202, 40–53, https://doi.org/10.1016/j.ecss.2017.12.006, 2018.

Sánchez-Garrido, J. C., and Nadal, I.: The Alboran Sea circulation and its biological response: A review, *Front. Mar. Sci.*, 9, 933390, https://doi.org/10.3389/fmars.2022.933390, 2022.

1025 Sánchez-Guillamón, O., Rueda, J. L., Wienberg, C., Ercilla, G., Vázquez, J. T., Gómez-Ballesteros, M., Urra, J., Moya-Urbano, E., Estrada, F., and Hebbeln, D.: Morphosedimentary, Structural and Benthic Characterization of Carbonate Mound Fields on the Upper Continental Slope of the Northern Alboran Sea (Western Mediterranean), *Geosciences*, 12, 111, https://doi.org/10.3390/geosciences12030111, 2022.

Sanchez-Vidal, A., Calafat, A., Canals, M., Frigola, J., and Fabres, J.: Particle fluxes and organic carbon balance 1030 across the Eastern Alboran Sea (SW Mediterranean Sea), *Cont. Shelf Res.*, 25, 609–628, https://doi.org/10.1016/j.csr.2004.11.004, 2005.

Schlager, W.: The paradox of drowned reefs and carbonate platforms, *GSA Bull.*, 92, 197–211, https://doi.org/10.1130/0016-7606(1981)92<197>2.0.Co;2, 1981.

Schlager, W.: Sedimentation rates and growth potential of tropical, cool-water and mud-mound carbonate 1035 systems, *Geol. Soc. Lond. Spec. Publ.*, 178, 217–227, https://doi.org/10.1144/GSL.SP.2000.178.01.14, 2000.

Schlager, W.: Benthic carbonate factories of the Phanerozoic, *Int. J. Earth Sci.*, 92, 445–464, https://doi.org/10.1007/s00531-003-0327-x, 2003.

Schmitz, O. J., Raymond, P. A., Estes, J. A., Kurz, W. A., Holtgrieve, G. W., Ritchie, M. E., Schindler, D. E., Spivak, A. C., Wilson, R. W., Bradford, M. A., Christensen, V., Deegan, L., Smetacek, V., Vanni, M. J., and 1040 Wilmers, C. C.: Animating the Carbon Cycle, *Ecosystems*, 17, 344–359, https://doi.org/10.1007/s10021-013-9715-7, 2014.

Schmitz, O. J., Wilmers, C. C., Leroux, S. J., Doughty, C. E., Atwood, T. B., Galetti, M., Davies, A. B., and Goetz, S. J.: Animals and the zoogeochemistry of the carbon cycle, *Science*, 362, 6419, https://doi.org/10.1126/science.aar3213, 2018.

1045 Smith, S. V., and Mackenzie, F. T.: The Role of CaCO3 Reactions in the Contemporary Oceanic CO2 Cycle, *Aquat. Geochem.*, 22, 153–175, https://doi.org/10.1007/s10498-015-9282-y, 2015.

Soetaert, K., Mohn, C., Rengstorf, A., Grehan, A., and van Oevelen, D.: Ecosystem engineering creates a direct nutritional link between 600-m deep cold-water coral mounds and surface productivity, *Sci Rep*, 6, 35057, https://doi.org/10.1038/srep35057, 2016.

1050 Stalder, C., El Kateb, A., Vertino, A., Rüggeberg, A., Camozzi, O., Pirkenseer, C. M., Spangenberg, J. E., Hajdas, I., Van Rooij, D., and Spezzaferri, S.: Large-scale paleoceanographic variations in the western Mediterranean Sea during the last 34,000 years: From enhanced cold-water coral growth to declining mounds, *Mar. Micropaleontol.*, 143, 46–62, https://doi.org/10.1016/j.marmicro.2018.07.007, 2018.

Stalling, D., Westerhoff, M., and Hege, H.-C.: Amira: a highly interactive system for visual data analysis, in 1055 Hansen, C. D. and Johnson, C. R. (eds.), *Visualization Handbook*, Butterworth-Heinemann, 749–LXXVIII, https://doi.org/10.1016/B978-012387582-2/50040-X, 2005.

Strong, J. A., Andonegi, E., Bizsel, K. C., Danovaro, R., Elliott, M., Franco, A., Garces, E., Little, S., Mazik, K., Moncheva, S., Papadopoulou, N., Patrício, J., Queirós, A. M., Smith, C., Stefanova, K., and Solaun, O.: Marine

biodiversity and ecosystem function relationships: The potential for practical monitoring applications, *Estuar. Coast. Shelf Sci.*, 161, 46–64, https://doi.org/10.1016/j.ecss.2015.04.008, 2015.

Tamborrino, L., Titschack, J., Wienberg, C., Purkis, S., Eberli, G. P., and Hebbeln, D.: Spatial distribution and morphometry of the Namibian coral mounds controlled by the hydrodynamic regime and outer-shelf topography, *Front. Mar. Sci.*, 9, 877616, https://doi.org/10.3389/fmars.2022.877616, 2022.

Tamborrino, L., Wienberg, C., Titschack, J., Wintersteller, P., Mienis, F., Schröder-Ritzrau, A., Freiwald, A., Orejas, C., Dullo, W.-C., Haberkern, J., and Hebbeln, D.: Mid-Holocene extinction of cold-water corals on the Namibian shelf steered by the Benguela oxygen minimum zone, *Geology*, 47, 1185–1188, https://doi.org/10.1130/g46672.1, 2019.

Thiem, Ø., Ravagnan, E., Fosså, J. H., and Berntsen, J.: Food supply mechanisms for cold-water corals along a continental shelf edge, *J. Mar. Syst.*, 60, 207–219, https://doi.org/10.1016/j.jmarsys.2005.12.004, 2006.

Titschack, J., Baum, D., De Pol-Holz, R., López Correa, M., Forster, N., Flögel, S., Hebbeln, D., Freiwald, A., and Riegl, B.: Aggradation and carbonate accumulation of Holocene Norwegian cold-water coral reefs, *Sedimentology*, 62, 1873–1898, https://doi.org/10.1111/sed.12206, 2015.

Titschack, J., Fink, H. G., Baum, D., Wienberg, C., Hebbeln, D., and Freiwald, A.: Mediterranean cold-water corals – an important regional carbonate factory?, *The Depositional Record*, 2, 74–96, https://doi.org/10.1002/dep2.14, 2016.

Titschack, J., Thierens, M., Dorschel, B., Schulbert, C., Freiwald, A., Kano, A., Takashima, C., Kawagoe, N., and Li, X.: Carbonate budget of a cold-water coral mound (Challenger Mound, IODP Exp. 307), *Mar. Geol.*, 259, 36–46, https://doi.org/10.1016/j.margeo.2008.12.007, 2009.

Wang, H., Lo Iacono, C., Wienberg, C., Titschack, J., and Hebbeln, D.: Cold-water coral mounds in the southern Alboran Sea (western Mediterranean Sea): Internal waves as an important driver for mound formation since the last deglaciation, *Mar. Geol.*, 412, 1–18, https://doi.org/10.1016/j.margeo.2019.02.007, 2019.

Wang, H., Titschack, J., Wienberg, C., Korpanty, C., and Hebbeln, D.: The Importance of Ecological Accommodation Space and Sediment Supply for Cold-Water Coral Mound Formation, a Case Study From the Western Mediterranean Sea, *Front. Mar. Sci.*, 8, 760909, https://doi.org/10.3389/fmars.2021.760909, 2021.

Wehrmann, L. M., Knab, N. J., Pirlet, H., Unnithan, V., Wild, C., and Ferdelman, T. G.: Carbon mineralization and carbonate preservation in modern cold-water coral reef sediments on the Norwegian shelf, *Biogeosciences*, 6, 663–680, https://doi.org/10.5194/bg-6-663-2009, 2009.

Wheeler, A. J., Beyer, A., Freiwald, A., de Haas, H., Huvenne, V. A. I., Kozachenko, M., Olu-Le Roy, K., and Opderbecke, J.: Morphology and environment of cold-water coral carbonate mounds on the NW European margin, *Int. J. Earth Sci.*, 96, 37–56, https://doi.org/10.1007/s00531-006-0130-6, 2007.

Wheeler, A. J., Kozachenko, M., Masson, D. G., and Huvenne, V. A. I.: Influence of benthic sediment transport on cold-water coral bank morphology and growth: the example of the Darwin Mounds, north-east Atlantic, *Sedimentology*, 55, 1875–1887, https://doi.org/10.1111/j.1365-3091.2008.00970.x, 2008.

Wienberg, C.: A Deglacial Cold-Water Coral Boom in the Alborán Sea: From Coral Mounds and Species Dominance, *Mediterr. Cold-Water Corals: Past, Present and Future Coral Reefs of the World*, 57–60, https://doi.org/10.1007/978-3-319-91608-8_7, 2019.

Wienberg, C., Freiwald, A., Frank, N., Mienis, F., Titschack, J., Orejas, C., and Hebbeln, D.: Cold-Water Coral Reefs in the Oxygen Minimum Zones Off West Africa, *Cold-Water Coral Reefs of the World Coral Reefs of the World*, 199–235, https://doi.org/10.1007/978-3-031-40897-7_8, 2023.

Wienberg, C., Krengel, T., Frank, N., Wang, H., Van Rooij, D., and Hebbeln, D.: Cold-water coral mounds in the western Mediterranean Sea: New insights into their initiation and development since the Mid-Pleistocene in

response to changes of African hydroclimate, *Quat. Sci. Rev.*, 293, 107723,
https://doi.org/10.1016/j.quascirev.2022.107723, 2022.

1105   Wienberg, C., and Titschack, J.: Framework-Forming Scleractinian Cold-Water Corals Through Space and
       Time: A Late Quaternary North Atlantic Perspective, in Rossi, S., Bramanti, L., Gori, A., and Orejas, C. (eds.),
       Marine Animal Forests, 699–732, https://doi.org/10.1007/978-3-319-17001-5_16-1, 2017.

       Wienberg, C., Titschack, J., Freiwald, A., Frank, N., Lundälv, T., Taviani, M., Beuck, L., Schröder-Ritzrau, A.,
       Krengel, T., and Hebbeln, D.: The giant Mauritanian cold-water coral mound province: Oxygen control on coral
       mound formation, *Quat. Sci. Rev.*, 185, 135–152, https://doi.org/10.1016/j.quascirev.2018.02.012, 2018.

1110   Wood, M., Hayes, C. T., and Paytan, A.: Global Quaternary Carbonate Burial: Proxy- and Model-Based
       Reconstructions and Persisting Uncertainties, *Ann. Rev. Mar. Sci.*, 15, 277–302, https://doi.org/10.1146/annurev-
       marine-031122-031137, 2023.

       Yin, S., Hernández-Molina, F. J., Fan, W., and Li, J.: Efficient organic carbon burial by bottom currents in the
       ocean: A potential role in climate modulation, *Geophys. Res. Lett.*, 51, e2024GL109444,
1115   https://doi.org/10.1029/2024GL109444, 2024.